IEEE Access
Multidisciplinary | Rapid Review | Open Access Journal

Received July 10, 2020, accepted July 21, 2020, date of publication August 3, 2020, date of current version August 20, 2020.

Digital Object Identifier 10.1109/ACCESS.2020.3013701

A Time Fractional Model of Generalized Couette Flow of Couple Stress Nanofluid With Heat and Mass Transfer: Applications in Engine Oil

FARHAD ALI[1,2], ZUBAIR AHMAD[3], MUHAMMAD ARIF[3], ILYAS KHAN[4], AND KOTTAKKARAN SOOPPY NISAR[5]

[1]Faculty of Mathematics and Statistics, Ton Duc Thang University, Ho Chi Minh City 700000, Vietnam
[2]Computational Analysis Research Group, Ton Duc Thang University, Ho Chi Minh City 700000, Vietnam
[3]Department of Mathematics, City University of Science and Information Technology, Peshawar 25000, Pakistan
[4]Department of Mathematics, College of Science Al-Zulfi, Majmaah University, Al Majmaah 11952, Saudi Arabia
[5]Department of Mathematics, College of Arts and Science, Prince Sattam Bin Abdulaziz University, Wadi Al-Dawasir 11991, Saudi Arabia

Corresponding author: Farhad Ali (farhad.ali@tdtu.edu.vn)

ABSTRACT The aim of this study is to obtain the closed form solutions for the laminar and unsteady couple stress fluid flow. The fluid is allowed to flow between two infinite parallel plates separated by distance ℓ. Moreover, we have considered that the lower plate is moving with uniform velocity U_0 and upper plate is stationary. For this purpose, engine oil is taken as a base fluid and to enhance the efficiency of lubricating oil, Molybdenum disulphide nanoparticles are dispersed uniformly in the engine oil. The flow is formulated mathematically in terms of partial differential equations of order four. Furthermore, the derived system of partial differential equations are fractionalized by using the mostly used definition of Caputo-Fabrizio time fractional derivative. The more general exact solutions for velocity, temperature and concentration distributions are obtained by using the joint applications of Fourier and the Laplace transforms. The effect of different parameters of interest of the obtained general solutions are discussed by sketching graphs. Furthermore, substituting favorable limits of different parameters, four different limiting cases are recovered from our obtained general solutions i.e. (a) Couette flow (b) Classical couple stress fluid (c) Newtonian viscous fluid and (d) in the absence of thermal and concentration. Moreover, the effect of different physical parameters on the velocity, temperature and concentration distributions are discussed graphically. It is worth noting that couple stress parameter corresponds to a decrease in the velocity profile. In order to observe the differences clearly, all the figures are compared for integer order and fractional order which provide a more realistic approach as compared to the classical model. Additionally, skin friction is calculated at lower as well as upper plate. Nusselt number and Sherwood number are also tabulated. It is noticed that the rate of heat transfer of engine oil can be enhanced up to 12.38% and decrease in mass transfer up to 2.14% by adding Molybdenum disulphide nanoparticles in regular engine oil.

INDEX TERMS Couple stress nanofluid (CSNF), Caputo-Fabrizo (CF), Fourier transform (FT), generalized Couette flow, Laplace transform (LT), Molybdenum disulphide (MoS_2).

I. INTRODUCTION

There are many fluids exists in the universe. These fluids are categorized within two main types based on their rheologies. The fluid which obey the Newton law of viscosity are Newtonian fluids while the others are non-Newtonian fluids. These fluids have many physical and real world applications such as industrial, medical and engineering processes. There are various physical phenomenon which cannot be explained by simple Newtonian viscous fluids. Non-Newtonian fluids are broadly used in different engineering and industrial problems. Furthermore, non-Newtonian fluids are further sub-classified into various types. Some real fluids such as polymeric fluids, colloidal suspensions, fluids containing additives and randomly oriented particles that cannot be described accurately by the classical Navier-Stokes' theory. To study the characteristics of these fluids, researchers proposed different models. For the first time, Stokes' [1] presented the idea of couple

The associate editor coordinating the review of this manuscript and approving it for publication was Lei Wang.

stress theory for the fluids which have different features from the classical Newtonian viscous fluids such as, existence of body couples and couple stresses. According to Stokes', couple stress fluid (CSF) is a simple generalization of the classical Newtonian viscous fluid theory with body couples, couple stresses and anti-symmetric stress tensor. These types of fluids contains random oriented and rigid particles. The main purpose of couple stresses is to present the size effect of these type of fluids which cannot be described accurately by classical viscous fluid theory. As described earlier that CSF are the fluids which consist of randomly oriented and rigid particles such as, Liquid crystals, lubrications, blood and so on. Due to the rotation of freely suspended particles, the spin field results an antisymmetric stress tensor named as couple stress, which leads us to the theory of couple stresses. The CSF model is more competent to clarify the behavior of various types of polymer suspensions, blood, lubricants, liquid crystals and so on. Some of the applications of CSF have been discussed in an another paper of Stokes' [2]. CSF model have many applications in modern world such as hydromagnetics, Pumping phenomenon, hemodynamics, blood diseases and blood in micro-circulatory systems [3]–[7]. Recently many researchers investigated CSF in their studies due to significance of these fluids. Hadjesfandiari and Dargush [8] examined several versions of CSF in their study. Tripathi [9] investigated CSF through a permeable medium with peristaltic hemodynamic and slip effect at the boundary. Devakar *et al*. [10] derived solutions of CSF flows with slip conditions. In their study, they discussed different cases (Poiseuille, Couette and generalized Couette flow). They concluded that couple stress parameter is responsible for retardation of fluid velocity. Ramanaiah [11] studied the squeeze films between a channel lubricated by CSF. From the results, he concluded that the squeeze time increases by taking CSF as a lubricant. Ramzan *et al.* [12] analyzed the solutions of three-dimensional CSF flow. They also discussed the CSF flow with the effect of Newtonian heating. Devi and Mahajan [13] discussed the global nonlinear stability of CSF. They also claimed that CSF is more stable than the Newtonian viscous fluid. Umavathi *et al.* [14] analyzed the solutions of laminar flow through channel occupied with CSF in a permeable medium. They also taken Darcy dissipation and viscous term in the energy field and discussed its effects graphically. Chippa and Sarangi [15] investigated the elastohydrodynamically lubricated finite line contact with the effect of CSF. They concluded from their study that CSF parameter increases thickness of the film which results less wear of direct metal to metal contact. They also claimed that coefficient of friction decreases by increasing CSF parameter which results to improve the performance of lubrication. Alsaedi *et al.* [16] studied the CSF incompressible flow over a porous medium. They also analyzed expressions of different parameters as a function of CSF parameter. Basha *et al.* [17] presented the numerical solutions for the transient two-dimensional natural convective CSF flow past over a vertical plate. Reddy *et al.* [18] investigated the solutions for hydromagnetic peristaltic motion of CSF through a porous channel. Awais *et al.* [19] analyzed CSF flow on a convective sliding surface. They also displayed the streamlines to differentiate CSF model from the classical Newtonian viscous fluid model. Makinde and Eegunjobi [20] presented the numerical solution of steady CSF flow in a vertical parallel plates stuff with porous substances. Farooq *et al.* [21] analysed the solutions for CSF flow through a channel. They discussed four different cases of the given flow i.e. both the plates are at rest, one plate is moving, both plates are moving, one plate is moving with external pressure gradient. Hayat *et al.* [22] investigated the melting heat transfer of CSF over a stretching sheet. They concluded that CSF parameter is accountable for the retardation of boundary layer thickness and velocity distribution and an reverse impact is experienced for temperature and surface heat transfer.

There are many physical problems that cannot be described through simple classical models. To study such type of problems, fractional calculus was introduced. The concept of fractional calculus was established after Leibniz presented the concept of nth order derivatives. Leibniz asked from Del Hospital that what will be the results if we consider fractional order. After that, numerous scientists starts thinking over it and they offered different representations of fractional derivatives [23]. The practical applications of fractional calculus can be seen in the modern technologies such as electrochemistry, electromagnetism, electric circuits, voltage divider, model of neurons, 3-D chaotic systems, chaotic circuits [24], [25], geotechnical engineering [26], quantum mechanics [27], Chaotic processes [28]. Some other electrochemical and biomedical applications are briefly discussed by Magin [29].

In the literature, there are many definitions of fractional model, but in the present study, we will use the newly presented definition of Caputo-Fabrizio time fractional derivative. In 2015, two mathematicians Michele Caputo and Mauro Fabrizio presented a new definition of fractional derivative with local kernel which was given with two various illustrations for the space and time variable [30]. In an another paper, they discussed some applications of their presented definition for fractional derivative [31]. Nowadays, most of the researchers are using CF fractional derivative because of their memory effect. The cause of using CF fractional derivative in our model is that as we have considered CSF in our study which is a viscoelastic non-Newtonian fluid. CF time fractional derivatives gives us more accurate and realistic results for viscoelastic fluids as compared to other fractional operators with the singular kernels. Akhtar [32] derived the solutions for the channel flow of CSF with C and CF time fractional derivatives and compare their results. According to him, the analysis shows that time fractional derivative is more dominant than the classical derivative. Arif *et al.* [33] calculated the exact solutions of CSF for generalized couette flow using CF fractional derivative. In an another paper, Arif *et al.* [34] investigated the solutions for

the heat transfer of CSF through a channel. Sheikh *et al.* [35] derived the closed form solutions for the CF fractional model of second-grade fluid flow over a fluctuating plate. Ali *et al.* [36] reported the solutions of Walters'-B fluid with the effect of MHD by considering CF time fractional derivative. Imran *et al.* [37] reported the solutions for the CF and AB frational model of MHD free convection flow of incompressible Newtonian viscous fluid passing over an inclined plate. Ahmad *et al.* [38] investigated the solutions for the heat and mass transfer of Jeffrey fluid flow over a vertical plate. They generalized the classical Jaffery fluid model with C and CF fractional model and compared the obtained results of both fractional operators. Khan *et al.* [39] generalized classical derivative by CF fractional derivative to investigate the results for casson fluid flow passing through a channel.

Nanofluid is a combination of solid nanoparticles suspended in the base fluids. Usually base fluids contains engine oil, ethylene glycol, water, crude oils etc. The solid nanoparticles that are suspended in the base fluids by many researchers are made of silver, copper, aluminum, graphite, molybdenum disulphide etc. From the beginning, scientists are trying to recover the efficiencies of different regular fluid. For this, in the beginning scientists and researchers used mili and micro-sized particles. Maxwell [40] gave the idea of using micro-sized particles within the base fluids but Maxwell's idea have some limitations. Later on, Choi and Eastman [41] was the first who utilized nano-sized particles in the base fluids. Choi's idea have some improvements, like less surface erosion, slow settling down, less clogging and sedimentation as compared to micro-sized particles. Many researchers found that using nanoparticles in the base fluids can boost up the thermal conductivity and heat transfer rate. For example, Reddy *et al.* [42] examined the dusty flow along a paraboloid revolution with the effect of silver, gold and platinum nanoparticles in the water base fluid. Arif *et al.* [43] investigate the heat transfer rate by adding graphene and molybdenum disulphide in the base fluid. They noticed that by adding these nanoparticles within the base fluids improved the characteristics of EO. Similarly, Ali *et al.* [44] suspended silver nanoparticles in the engine oil base fluid. They noticed that by increasing the amount of nanoparticles, the collision of nanoparticles rises which results to boost up the heat transfer rate up to 15%. Mahian *et al.* [45] explained some applications of nanofluids in solar energy such as solar radiators, pools, thermoelectric cells etc. Some applications of nanofluids in nuclear reactors, electronics, transportation, biomedicines and smart fluid devices such as laptops, computers and smart phones are examined by Wong and De Leon [46]. Some other practical applications of nanofluids in modern technologies are in automobiles [47], transformer oil [48], production of antibacterial [49], cooling systems [50] etc.

Nowadays, different nanoparticles are using with in different base fluids [51]–[53]. In the present work, we have considered Engine oil (EO) as a base fluid and spherical shaped Molybednum Disulphide (MoS_2) as nanoparticles due to low friction properties and higher thermal conductivity are dispersed in it, which will boost the heat transfer rate and increase lubricity of the EO. There are two main causes of choosing EO and MoS_2. The first cause of choosing MoS_2 and EO is that this type of experiment will be less expensive. Because by taking platinum, gold or other type of nanoparticle are more expensive as compared to the considered nanoparticles. The other cause is that, MoS_2 is used as a dry lubricant. Therefore MoS_2 will decrease the friction of the EO which results to increase the lubricity of regular engine oil with less erosion of surfaces and channels [54]. Jan *et al.* [55] obtained the exact solutions of EO based Brinkman-type fluid over a moving porous plate with spherical shape MoS_2 nanoparticles. They noticed an increase in rate of heat transfer of the nanofluid by increasing amount of nanoparticles. Ali *et al.* [56] investigated the influence of various shapes of MoS_2 nanoparticles on the flow of EO based brinkman-type fluid. In their study, they examined the impact of four different shaped nanoparticles i.e. blade, platelet, brick and cylinder shape. They noticed that blade and platelet shaped nanoparticles has more thermal conductivity than that of cylindrical and brick shaped nanoparticles and can improve the rate of heat transfer up to 13.51%.

The mutual study of mass and heat transfer have taken a great attention of the scientists. The joint existence of heat and mass transfer appear due to the joint effect of thermal bouncy diffusion. Different applications of this phenomenon can be seen in modern technologies and industries such as food processing, solar collectors, cooling processes, different lubricants such as engine oil etc. [57]–[59]. Reddy and Firdows [60] investigated the heat and mass transfer phenomena of micropolar dusty fluid across a paraboloid revolution. In an another paper, Reddy *et al.* [61] analysed the solutions for the heat and mass transfer of three dimensional flow of hydromagnetic Carreau nanofluid transport over a stretching sheet.

The flow inside two parallel plates is a type of open channel flow. Open channel flow has wide applications in the natural and artificial phenomenon. The flow of canal, river etc. with a free surface are the examples of open channel flow. The flow between two parallel plates which are both stationary is called is known as poiseuille flow. The flow in which one or both of the plates sliding with some constant velocity is named as couette flow. The couette flow with the effect of external pressure gradient becomes generalized couette flow. Generalized couette flow have wide applications in industrial as well as in modern sciences. Arif *et al.* [33] derived the solutions of CSF flow for generalized couette flow. From their results, they noticed that CSF velocity is less as compared to classical Newtonian viscous fluid velocity. Devakar *et al.* [62] analyzed generalized couette flow of CSF through a channel. They claimed that CSF parameter decreases the magnitude of velocity profile.

Motivated from the above mentioned literature, in this study, we discuss the unsteady flow of CSNF through an open channel. The flow of CSNF is considered through a

horizontal channel. The lower plate is sliding with constant velocity U_0 while the upper plate is taken at rest. External pressure gradient is considered in the axis of the fluid flow. Furthermore, the base fluid is selected as a EO and MoS_2 nanoparticles are equally dispersed within the EO to enhance the thermal conductivity and heat transfer rate. Classical derivative is fractionalized by considering CF fractional derivative. To obtain the exact solutions, integral transforms are used. The obtained results is presented through figures. The influence of different parameters of interest on the CSNF flow are displayed. Finally, the skin friction is evaluated for momentum equation, Nusselt number is evaluated from the temperature profile and Sherwood number is evaluated from the concentration profile. The effect of various embedded parameters on skin friction, Nusselt number and Sherwood number is also discussed.

II. PROBLEM FORMULATION

In this article, we have considered the laminar and unsteady flow of CSNF between two parallel plates separated by a distance ℓ. The motion of the fluid is considered in x direction. The system of equations which governs the CSNF flow is given as [32]–[34]:

$$\nabla \cdot \vec{V} = 0, \tag{1}$$

$$\begin{aligned}\rho_{nf}\frac{D\vec{V}}{Dt_1^*} &= -\nabla p - \mu_{nf}\nabla\times\nabla\times\vec{V}\\ &\quad -\eta*\nabla\times\nabla\times\nabla\times\nabla\times\vec{V}\\ &\quad +\vec{g}\,(\rho\beta_T)_{nf}\left(T_1^*-T_{1\infty}^*\right)\\ &\quad +\vec{g}\,(\rho\beta_C)_{nf}\left(C_1^*-C_{1\infty}^*\right)+\rho\vec{b}_1,\end{aligned} \tag{2}$$

$$\left(\rho c_p\right)_{nf}\frac{\partial\vec{T}}{\partial t_1^*} = k_{nf}\nabla\times\nabla\times\vec{T}, \tag{3}$$

$$\frac{\partial\vec{C}}{\partial t_1^*} = D_{nf}\nabla\times\nabla\times\vec{C}. \tag{4}$$

Here $\vec{V}$, $\vec{T}$ and $\vec{C}$ are the velocity, temperature and concentration vectors of the fluid respectively. p, μ_{nf}, $\eta*$, $\vec{g}$, $\vec{b}_1$, β_T, β_C, $\left(\rho c_p\right)_{nf}$, k_{nf}, and D_{nf} is the constant external pressure, dynamic viscosity, couple stress parameter, gravitational acceleration, body forces vector, thermal expansion coefficient, concentration coefficient, specific heat, thermal conductivity and thermal diffusivity of nanofluid. The velocity, temperature and concentration fields of the given flow regime are as under:

$$\left.\begin{aligned}\vec{V} &= \left(u_1^*(y_1^*,t_1^*),0,0\right),\\ \vec{T} &= \left(T_1^*(y_1^*,t_1^*),0,0\right),\\ \vec{C} &= \left(C_1^*(y_1^*,t_1^*),0,0\right),\end{aligned}\right\}. \tag{5}$$

Using equation (5), equation (1) automatically satisfies and equations (2-4) in components form takes the shape:

$$\begin{aligned}\rho_{nf}\frac{\partial u_1^*\left(y_1^*,t_1^*\right)}{\partial t_1^*} &= -\frac{\partial p}{\partial x_1^*}+\mu_{nf}\frac{\partial^2 u\left(y_1^*,t_1^*\right)}{\partial y_1^{*2}}\\ &\quad -\eta*\frac{\partial^4 u_1^*\left(y_1^*,t_1^*\right)}{\partial y_1^{*4}}+g_x\,(\rho\beta_T)_{nf}\left(T_1^*-T_{1\infty}^*\right)\\ &\quad +g_x\,(\rho\beta_C)_{nf}\left(C_1^*-C_{1\infty}^*\right)+\rho\vec{b}_1,\end{aligned} \tag{6}$$

$$\begin{aligned}\left(\rho c_p\right)_{nf}\frac{\partial T_1^*\left(y_1^*,t_1^*\right)}{\partial t_1^*} &= k_{nf}\frac{\partial^2 T_1^*\left(y_1^*,t_1^*\right)}{\partial y_1^{*2}},\end{aligned} \tag{7}$$

$$\begin{aligned}\frac{\partial C_1^*\left(y_1^*,t_1^*\right)}{\partial t_1^*} &= D_{nf}\frac{\partial^2 C_1^*\left(y_1^*,t_1^*\right)}{\partial y_1^{*2}}.\end{aligned} \tag{8}$$

A. GENERALIZED COUETTE FLOW

The fluid flow through a channel in which one plate is at rest and the other plate moves at a constant velocity with external pressure gradient along the direction of flow is considered as generalized Couette flow.

Initially, for $t_1^* \le 0$ the fluid and both the plates are at rest with ambient temperature $T_{1\infty}^*$ and constant concentration $C_{1\infty}^*$. At $t_1^* = 0^+$, the lower plate starts moving with constant velocity $U_0H\left(t_1^*\right)$ while the upper plate remains static. The temperature and concentration of the lower plate raised to T_{1w}^* and C_{1w}^* respectively and then remains constant while the upper plate remains at ambient temperature $T_{1\infty}^*$ and constant concentration $C_{1\infty}^*$.

The system of equation which govern the CSNF flow under the above assumptions along with initial and boundary conditions are given as [32]–[34]:

$$\begin{aligned}\rho_{nf}\frac{\partial u_1^*\left(y_1^*,t_1^*\right)}{\partial t_1^*} &= G^*+\mu_{nf}\frac{\partial^2 u_1^*\left(y_1^*,t_1^*\right)}{\partial y_1^{*2}}\\ &\quad -\eta\frac{\partial^4 u_1^*\left(y_1^*,t_1^*\right)}{\partial y_1^{*4}}+g_x\,(\rho\beta_T)_{nf}\left(T_1^*-T_{1\infty}^*\right)\\ &\quad +g_x\,(\rho\beta_C)_{nf}\left(C_1^*-C_{1\infty}^*\right),\end{aligned} \tag{9}$$

$$\begin{aligned}\left(\rho c_p\right)_{nf}\frac{\partial T_1^*\left(y_1^*,t_1^*\right)}{\partial t_1^*} &= k_{nf}\frac{\partial^2 T_1^*\left(y_1^*,t_1^*\right)}{\partial y_1^{*2}},\end{aligned} \tag{10}$$

$$\begin{aligned}\frac{\partial C_1^*\left(y_1^*,t_1^*\right)}{\partial t_1^*} &= D_{nf}\frac{\partial^2 C_1^*\left(y_1^*,t_1^*\right)}{\partial y_1^{*2}},\end{aligned} \tag{11}$$

with the physical initial and boundary conditions in (12), as shown at the bottom of the next page. For nanofluids, the expressions for ρ_{nf}, μ_{nf}, $\left(\rho c_p\right)_{nf}$, $(\rho\beta_T)_{nf}$,

$(\rho\beta_C)_{nf}$, k_{nf} and D_{nf} are given by [49]–[51]:

$$\left.\begin{aligned}
&\rho_{nf} = \rho_f\left((1-\phi)+\frac{\phi\rho_s}{\rho_f}\right), \mu_{nf} = \mu_f\left(\frac{1}{(1-\phi)^{2.5}}\right),\\
&(\rho\beta_T)_{nf} = (\rho\beta_T)_f\left((1-\phi)+\frac{\phi(\rho\beta_T)_s}{(\rho\beta_T)_f}\right),\\
&(\rho\beta_C)_{nf} = (\rho\beta_C)_f\left((1-\phi)+\frac{\phi(\rho\beta_C)_s}{(\rho\beta_C)_f}\right),\\
&\left(\rho c_p\right)_{nf} = \left(\rho c_p\right)_f\left((1-\phi)+\frac{\phi(\rho c_p)_s}{(\rho c_p)_f}\right),\\
&k_{nf} = k_f\left[\frac{2k_f+k_s-2\phi(k_f-k_s)}{2k_f+k_s+2\phi(k_f-k_s)}\right],\\
&D_{nf} = (1-\phi)D_f, \lambda_{nf} = \frac{k_{nf}}{k_f},
\end{aligned}\right\} \tag{13}$$

where $\rho_f, \mu_f, \beta_f, k_f$ and D_f is the density, dynamic viscosity, thermal expansion coefficient, thermal conductivity and thermal diffusivity of the base fluid respectively. Similarly ρ_s, μ_s, β_s and k_s is the density, dynamic viscosity, thermal expansion coefficient, thermal conductivity and thermal diffusivity of the solid nanoparticles respectively.

The following non-dimensional variables will be used for the dimensional analysis of the governing equations:

$$\left.\begin{aligned}
&\xi = \frac{y_1^*}{\ell}, \Psi = \frac{u_1^*}{U_0}, \tau = \frac{U_0 t_1^*}{\ell}, \lambda = \frac{\eta^*}{\mu\ell^2},\\
&P = \frac{\ell^2}{\mu_{nf}U_0}G^*, \Theta = \frac{T_1^*-T_{1\infty}^*}{T_{1w}^*-T_{1\infty}^*}, \Phi = \frac{C_1^*-C_{1\infty}^*}{C_{1w}^*-C_{1\infty}^*},
\end{aligned}\right\}. \tag{14}$$

By using these dimensionless quantities, The dimensionless form of equations (9)-(12) along with initial and boundary conditions is given by:

$$\psi_1\frac{\partial\Psi(\xi,\tau)}{\partial\tau} = P+\frac{\partial^2\Psi(\xi,\tau)}{\partial\xi^2} - \lambda\frac{\partial^4\Psi(\xi,\tau)}{\partial\xi^4} + A_0\Theta(\xi,\tau)+A_1\Phi(\xi,\tau), \tag{15}$$

$$\psi_2\frac{\partial\Theta(\xi,\tau)}{\partial\tau} = \frac{\partial^2\Theta(\xi,\tau)}{\partial\xi^2}, \tag{16}$$

$$\psi_3\frac{\partial\Phi(\xi,\tau)}{\partial\tau} = \frac{\partial^2\Phi(\xi,\tau)}{\partial\xi^2}, \tag{17}$$

$$\left.\begin{aligned}
&\Psi(\xi,0)=0, \Theta(\xi,0)=0, \Phi(\xi,0)=0, \text{for } 0\le\xi\le\ell\\
&\Psi(0,\tau)=1, \Theta(0,\tau)=1, \Phi(0,\tau)=1, \text{for } \tau>0,\\
&\Psi(\ell,\tau)=0, \Theta(\ell,\tau)=0, \Phi(\ell,\tau)=0, \text{for } \tau>0,\\
&\frac{\partial^2\Psi(0,\tau)}{\partial\xi^2} = \frac{\partial^2\Psi(\ell,\tau)}{\partial\xi^2} = 0, \text{for } \tau>0,
\end{aligned}\right\} \tag{18}$$

here

$$\psi_1 = \varphi_0\varphi_1\mathrm{Re}, \psi_2 = \frac{\mathrm{Re}\,\mathrm{Pr}\,\varphi_5}{\varphi_4}, \psi_3 = \frac{\varphi_0}{Sc\mathrm{Re}},$$
$$\varphi_0 = (1-\phi)^{2.5}, \varphi_1 = (1-\phi)+\frac{\phi\rho_s}{\rho_f},$$
$$\varphi_2 = (1-\phi)+\frac{\phi(\rho\beta_T)_s}{(\rho\beta_T)_f}, \varphi_3 = (1-\phi)+\frac{\phi(\rho\beta_C)_s}{(\rho\beta_C)_f},$$
$$\varphi_4 = (1-\phi)+\frac{\phi\left(\rho c_p\right)_s}{\left(\rho c_p\right)_f}, \varphi_5 = \frac{2k_f+k_s-2\phi\left(k_f-k_s\right)}{2k_f+k_s+2\phi\left(k_f-k_s\right)}$$
$$A_0 = Gr\varphi_0\varphi_2, Gr = \frac{g_x(\beta_T)_f\ell^2\left(T_{1w}^*-T_{1\infty}^*\right)}{U_0\mu_f},$$
$$A_1 = Gm\varphi_0\varphi_3, Gm = \frac{g_x(\beta_C)_f\ell^2\left(C_{1w}^*-C_{1\infty}^*\right)}{U_0\mu_f},$$
$$\mathrm{Pr} = \frac{\left(\mu c_p\right)_f}{k_f}, \mathrm{Re} = \frac{U_0\ell}{\upsilon_f}, Sc = \frac{\upsilon_f}{D_f},$$

where Pr, Re, Sc, Gr, Gm, λ and P represents Prandtl number, Reynolds number, Schmidt number, thermal and mass Grashof numbers, dimensionless couple stress parameter and constant external pressure gradient.

III. EXACT SOLUTIONS USING CAPUTO-FABRIZIO FRACTIONAL DERIVATIVES

Applying the definition of Caputo-Fabrizio fractional derivative to the governing equations, the following time fractional CSNF model with fractional operator α will be obtained:

$${}^{CF}D_\tau^\alpha\psi_1\Psi(\xi,\tau) = P+\frac{\partial^2\Psi(\xi,\tau)}{\partial\xi^2} - \lambda\frac{\partial^4\Psi(\xi,\tau)}{\partial\xi^4}+A_0\Theta(\xi,\tau)+A_1\Phi(\xi,\tau), \tag{19}$$

$${}^{CF}D_\tau^\alpha\psi_2\Theta(\xi,\tau) = \frac{\partial^2\Theta(\xi,\tau)}{\partial\xi^2}, \tag{20}$$

$${}^{CF}D_\tau^\alpha\psi_3\Phi(\xi,\tau) = \frac{\partial^2\Phi(\xi,\tau)}{\partial\xi^2}, \tag{21}$$

here ${}^{CF}D_\tau^\alpha$ is the definition of CF fractional derivatives with fractional parameter α which is defined as [30]:

$${}^{CF}D_\tau^\alpha g(\tau) = \frac{\mathrm{N}(\alpha)}{(1-\alpha)}\int_0^t e^{-\frac{\alpha(\tau-t)}{1-\alpha}}g'(\tau)dt, \tag{22}$$

where $\mathrm{N}(\alpha)$ is a normalization function such that $\mathrm{N}(0) = \mathrm{N}(1) = 1$ and $\alpha\in(0,1)$.

A. SOLUTIONS OF ENERGY EQUATION

By applying Laplace transform technique (LT) to equation (20) and incorporating equation (18), we get:

$$\frac{qL_1\psi_2\bar{\Theta}(\xi,s)}{(s+L_2)} = \frac{d^2\bar{\Theta}(\xi,s)}{d\xi^2}, \tag{23}$$

$$\left.\begin{aligned}
&u_1^*(y_1^*,0)=0, T_1^*(y_1^*,0)=T_{1\infty}^*, C_1^*(y_1^*,0)=C_{1\infty}^*, \text{for } 0\le y_1^*\le\ell \text{ and } t_1^*=0,\\
&u_1^*(0,t_1^*)=H(t_1^*)U_0,\ T_1^*(0,t_1^*)=T_{1w}^*, C_1^*(0,t_1^*)=C_{1w}^*, \text{for } t_1^*>0,\\
&u_1^*(\ell,t_1^*)=0, T_1^*(\ell,t_1^*)=T_{1\infty}^*, C_1^*(\ell,t_1^*)=C_{1\infty}^*, \text{for } t_1^*>0,\\
&\frac{\partial^2u_1^*(0,t_1^*)}{\partial y_1^{*2}} = \frac{\partial^2u_1^*(\ell,t_1^*)}{\partial y_1^{*2}} = 0, \text{for } t_1^*>0.
\end{aligned}\right\} \tag{12}$$

Similarly the transformed form of equation (18):

$$\left.\begin{array}{l}\bar{\Psi}(0,s)=\frac{1}{s},\bar{\Theta}(0,s)=\frac{1}{s},\bar{\Phi}(0,s)=\frac{1}{s},\text{for s}>0,\\ \bar{\Psi}(\ell,s)=0,\bar{\Theta}(\ell,s)=0,\bar{\Phi}(\ell,s)=0,\text{for s}>0,\\ \frac{d^2\bar{\Psi}(0,s)}{d\xi^2}=\frac{d^2\bar{\Psi}(\ell,s)}{d\xi^2}=0,\text{for s}>0,\end{array}\right\}. \tag{24}$$

To apply the finite sine Fourier transform [63], [64], we multiply both sides of equation (23) by $\sin\left(\frac{k\pi\xi}{\ell}\right)$ and taking integration with limits from 0 to ℓ w.r.t ξ and using equation (24), we get:

$$\bar{\Theta}_{FT}(k,s)=\frac{\chi_k}{s}\left(\frac{\psi_2(s+L_2)}{s\left(L_1+\psi_2\chi_k^2\right)+\psi_2\chi_k^2L_2}\right), \tag{25}$$

which implies

$$\bar{\Theta}_{FT}(k,s)=\frac{L_4(s+L_2)}{s(s+L_3)}. \tag{26}$$

By partial fraction w.r.t s and after some calculations, equation (26) can be written as:

$$\bar{\Theta}_{FT}(k,s)=\frac{L_2L_4}{sL_3}+\frac{L_4L_5}{s+L_3}. \tag{27}$$

By inverting LT, Equation (27) takes the following shape:

$$\Theta_{FT}(k,\tau)=\frac{L_2L_4}{L_3}+L_4L_5\exp(-L_3\tau), \tag{28}$$

here,

$$L_1=\frac{1}{1-\alpha},L_2=\frac{\alpha}{1-\alpha},\chi_k=\frac{k\pi\xi}{\ell},$$

$$L_3=\frac{\psi_2\chi_k^2L_2}{L_1+\psi_2\chi_k^2},\quad L_4=\frac{\psi_2\chi_k}{L_1+\psi_2\chi_k^2},L_5=1-\frac{L_2}{L_3}. \tag{29}$$

By applying inverse finite sine-Fourier transform to equation (29), final results takes the form:

$$\Theta(\xi,\tau)=1-\frac{\xi}{\ell}+\frac{2}{\ell}\sum_{k=1}^{\infty}L_4L_5\sin\left(\frac{k\pi\xi}{\ell}\right)\exp(-L_3\tau). \tag{30}$$

B. SOLUTIONS OF CONCENTRATION EQUATION

By applying LT to equation (21) and incorporating equation (18), we get:

$$\frac{sL_1\psi_3\bar{\Phi}(\xi,s)}{(s+L_2)}=\frac{d^2\bar{\Phi}(\xi,s)}{d\xi^2}, \tag{31}$$

By applying the finite sine Fourier transform on equation (31) and using equation (24), we get:

$$\bar{\Phi}_{FT}(k,s)=\frac{\chi_k}{s}\left(\frac{\psi_3(s+L_2)}{s\left(L_1+\psi_3\chi_k^2\right)+\psi_3\chi_k^2L_2}\right), \tag{32}$$

which implies that

$$\bar{\Phi}_{FT}(k,s)=\frac{L_7(s+L_2)}{s(s+L_6)}. \tag{33}$$

By partial fraction and after some calculations, we get the following results:

$$\bar{\Phi}_{FT}(k,s)=\frac{L_2L_7}{sL_6}+\frac{L_7L_8}{s+L_6}, \tag{34}$$

By inverting LT, equation (34) takes the shape:

$$\Phi_{FT}(k,\tau)=\frac{L_2L_7}{L_6}+L_7L_8\exp(-L_6\tau), \tag{35}$$

here,

$$L_6=\frac{\psi_3\chi_k^2L_2}{L_1+\psi_3\chi_k^2},\quad L_7=\frac{\psi_3\chi_k}{L_1+\psi_3\chi_k^2},L_8=1-\frac{L_2}{L_6}. \tag{36}$$

By inverting finite sine-Fourier transform, we obtain final results in the following form:

$$\Phi(\xi,\tau)=1-\frac{\xi}{\ell}+\frac{2}{\ell}\sum_{k=1}^{\infty}L_7L_8\sin\left(\frac{k\pi\xi}{\ell}\right)\exp(-L_6\tau). \tag{37}$$

C. SOLUTIONS OF MOMENTUM EQUATION

Applying LT to equation (19) and incorporating equation (18), we get:

$$\begin{aligned}&\frac{sL_1\psi_1\bar{\Psi}(\xi,s)}{(s+L_2)}\\&=\frac{P}{s}+\frac{d^2\bar{\Psi}(\xi,s)}{d\xi^2}\\&\quad-\lambda\frac{d^4\bar{\Psi}(\xi,s)}{d\xi^4}+A_0\bar{\Theta}(\xi,s)+A_1\bar{\Phi}(\xi,s).\end{aligned} \tag{38}$$

Now applying finite sine Fourier transform on equation (38) and incorporating equation (24), we get:

$$\begin{aligned}&\frac{sL_1\psi_1\bar{\Psi}_{FT}(k,s)}{(s+L_2)}\\&=\frac{P\left(1-(-1)^k\right)}{s\chi_k}\\&\quad+\frac{\chi_k}{s}-\chi_k^2\bar{\Psi}_{FT}(k,s)+\lambda\frac{\chi_k^3}{s}\\&\quad-\lambda\chi_k^4\bar{\Psi}_{FT}(k,s)+A_0\bar{\Theta}_{FT}(k,s)+A_1\bar{\Phi}_s(k,s).\end{aligned} \tag{39}$$

Alternatively, we can write:

$$\begin{aligned}\bar{\Psi}_{FT}(k,s)=&\left(\begin{array}{l}\left(\frac{P\left(1-(-1)^k\right)+\chi_k^2+\lambda\chi_k^4}{s\chi_k}\right)\\+A_0\bar{\Theta}_{FT}(k,s)+A_1\bar{\Phi}_{FT}(k,s)\end{array}\right)\\&\times\left(\frac{(s+L_2)}{\left(\psi_1L_1+\chi_k^2+\lambda\chi_k^4\right)(s+L_9)}\right),\end{aligned} \tag{40}$$

where $L_9=\frac{L_2\left(\chi_k^2+\lambda\chi_k^4\right)}{\left(\psi_1L_1+\chi_k^2+\lambda\chi_k^4\right)}$.

Now by incorporating $\bar{\Theta}_{FT}(k,s)$ and $\bar{\Phi}_{FT}(k,s)$ from equation (26) and equation (33), equation (40) becomes:

$$\bar{\Psi}_{FT}(k,s) = \left(\begin{array}{l}\left(\frac{P\left(1-(-1)^k\right)+\chi_k^2+\lambda\chi_k^4}{s\chi_k}\right)\\ +A_0\frac{L_4(s+L_2)}{s(s+L_3)}+A_1\frac{L_7(s+L_2)}{s(s+L_6)}\end{array}\right)\times\left(\frac{(s+L_2)}{\left(\psi_1L_1+\chi_k^2+\lambda\chi_k^4\right)(s+L_9)}\right). \quad (41)$$

Separation of RHS of equation (41) by using partial fraction w.r.t. s, we get:

$$\begin{aligned}&\bar{\Psi}_{FT}(k,s)\\ &=\left(\frac{P\left(1-(-1)^k\right)+\chi_k^2+\lambda\chi_k^4}{s\chi_k\left(\chi_k^2+\lambda\chi_k^4\right)}\right)\\ &+\left(\frac{P\left(1-(-1)^k\right)+\chi_k^2+\lambda\chi_k^4}{\chi_k\left(\psi_1L_1+\chi_k^2+\lambda\chi_k^4\right)(s+L_9)}\right)\\ &-\left(\frac{P\left(1-(-1)^k\right)+\chi_k^2+\lambda\chi_k^4}{\chi_k\left(\chi_k^2+\lambda\chi_k^4\right)(s+L_9)}\right)\\ &+\frac{A_0L_4}{\left(\psi_1L_1+\chi_k^2+\lambda\chi_k^4\right)}\\ &\times\left(\frac{L_2}{L_3s}+\frac{2L_5}{s+L_3}+\frac{2L_5(L_2-L_3)}{(s+L_3)^2}\right)\\ &+\frac{A_1L_7}{\left(\psi_1L_1+\chi_k^2+\lambda\chi_k^4\right)}\\ &\times\left(\frac{L_2}{L_6s}+\frac{2L_8}{s+L_6}+\frac{2L_8(L_2-L_6)}{(s+L_6)^2}\right). \quad (42)\end{aligned}$$

Inverting the Laplace transform, we get:

$$\begin{aligned}&\Psi_{FT}(k,\tau)\\ &=\left(\frac{P\left(1-(-1)^k\right)+\chi_k^2+\lambda\chi_k^4}{\chi_k\left(\chi_k^2+\lambda\chi_k^4\right)}\right)\\ &+\left(\frac{P\left(1-(-1)^k\right)+\chi_k^2+\lambda\chi_k^4}{\chi_k\left(\psi_1L_1+\chi_k^2+\lambda\chi_k^4\right)}\exp\left(-L_9\tau\right)\right)\\ &-\left(\frac{P\left(1-(-1)^k\right)+\chi_k^2+\lambda\chi_k^4}{\chi_k\left(\delta_k^2+\lambda\chi_k^4\right)}\exp\left(-L_9\tau\right)\right)\\ &+\frac{A_oL_4}{\left(\psi_1L_1+\chi_k^2+\lambda\chi_k^4\right)}\\ &\times\left(\begin{array}{l}\frac{L_2}{L_3}+2L_5\exp\left(-L_3\tau\right)\\ +2L_5\left(L_2-L_3\right)\tau\exp\left(-L_3\tau\right)\end{array}\right)\\ &+\frac{A_1L_7}{\left(\psi_1L_1+\chi_k^2+\lambda\chi_k^4\right)}\\ &\times\left(\begin{array}{l}\frac{L_2}{L_6}+2L_8\exp\left(-L_6\tau\right)\\ +2L_8\left(L_2-L_6\right)\tau\exp\left(-L_6\tau\right)\end{array}\right), \quad (43)\end{aligned}$$

or equalently:

$$\Psi_{FT}(k,\tau) = \left(\begin{array}{l}\frac{\left(1-(-1)^k\right)}{\chi_k}+\frac{(-1)^k}{\chi_k}-\frac{P\left(1-(-1)^k\right)}{\chi_k}\\ +\frac{P\left(1-(-1)^k\right)}{\chi_k^3}+\frac{P\left(1-(-1)^k\right)}{\left(1+\chi_k^2\right)}\end{array}\right)$$
$$+\left(\alpha_k-\beta_k\right)\exp\left(-L_9\tau\right)$$
$$+\delta_kA_0\exp\left(-L_3\tau\right)+\gamma_kA_1\exp\left(-L_6\tau\right). \quad (44)$$

By Applying inverse Finite Sine-Fourier transform to equation (44), we obtain the following results:

$$\Psi(\xi,\tau) = \left(\begin{array}{l}1-P-\left(\frac{1}{\ell}-\frac{P\ell}{2}\right)\xi\\ -\frac{P}{2}\xi^2+P\left(\frac{\cosh\left(\frac{\ell}{2}-\xi\right)}{osh\left(\frac{\ell}{2}\right)}\right)\end{array}\right)$$
$$+\left(\begin{array}{l}\frac{2}{\ell}\sum_{k=1}^{\infty}\left[\left(\alpha_k-\beta_k\right)e^{-L_9\tau}\right]\sin\left(\chi_k\xi\right)\\ +\frac{2}{\ell}\sum_{k=1}^{\infty}\left[\delta_kA_0e^{-L_3\tau}\right]\sin\left(\chi_k\xi\right)\\ +\frac{2}{\ell}\sum_{k=1}^{\infty}\left[\gamma_kA_1e^{-L_6\tau}\right]\sin\left(\chi_k\xi\right)\end{array}\right), \quad (45)$$

where

$$\begin{aligned}\alpha_k &= \left(\frac{P\left(1-(-1)^k\right)+\chi_k^2+\lambda\chi_k^4}{\delta_k\left(\psi_1L_1+\delta_k^2+\lambda\delta_k^4\right)}\right),\\ \beta_k &= \left(\frac{P\left(1-(-1)^k\right)+\chi_k^2+\lambda\chi_k^4}{\chi_k\left(\delta_k^2+\lambda\chi_k^4\right)}\right),\\ \delta_k &= \frac{L_4}{\left(\psi_1L_1+\chi_k^2+\lambda\chi_k^4\right)}\left(\frac{L_2}{L_3}+2L_5+2L_5\left(L_2-L_3\right)\tau\right),\\ \gamma_k &= \frac{L_7}{\left(\psi_1L_1+\chi_k^2+\lambda\chi_k^4\right)}\left(\frac{L_2}{L_6}+2L_8+2L_8\left(L_2-L_6\right)\tau\right).\end{aligned} \quad (46)$$

where equation (45) is the total solution which is the combination of unsteady and steady state solutions. The steady state solutions $\Psi_S(\xi)$ is given by:

$$\Psi_S(\xi) = 1-P-\left(\frac{1}{\ell}-\frac{P\ell}{2}\right)\xi - \frac{P}{2}\xi^2+G\left(\frac{\cosh\left(\frac{\ell}{2}-\xi\right)}{\cosh\left(\frac{\ell}{2}\right)}\right), \quad (47)$$

and the unsteady solutions $\Psi_\tau(\xi,\tau)$ is given by:

$$\begin{aligned}\Psi_\tau(\xi,\tau) &= \frac{2}{\ell}\sum_{k=1}^{\infty}\left[\left(\alpha_k-\beta_k\right)\exp\left(-L_9\tau\right)\right]\sin\left(\chi_k\xi\right)\\ &+\frac{2}{\ell}\sum_{k=1}^{\infty}\left[\delta_kA_0\exp\left(-L_3\tau\right)\right]\sin\left(\chi_k\xi\right)\\ &+\frac{2}{\ell}\sum_{k=1}^{\infty}\left[\gamma_kA_1\exp\left(-L_6\tau\right)\right]\sin\left(\chi_k\xi\right).\end{aligned} \quad (48)$$

IV. SPECIAL CASES

The present obtained general solutions are reduced to the following special cases:

A. NEWTONIAN VISCOUS FLUID FLOW

By putting $(\lambda=0)$, $(Gr=0)$ and $(Gm=0)$ in equation (15), we get the dimensionless form of couple stress

nanofluid in the following form:

$$B\frac{\partial \Psi(\xi,\tau)}{\partial \tau} = P + \frac{\partial^2 \Psi(\xi,\tau)}{\partial \xi^2}. \tag{49}$$

Applying the CF fractional derivative definition to equation (49), we obtain:

$${}^{CF}D_{\tau}^{\alpha} B\Psi(\xi,\tau) = P + \frac{\partial^2 \Psi(\xi,\tau)}{\partial \xi^2}. \tag{50}$$

By applying Laplace transform technique, we get,

$$\frac{sL_1 B\bar{\Psi}(\xi,s)}{(s+L_2)} = \frac{P}{s} + \frac{d^2\bar{\Psi}(\xi,s)}{d\xi^2}. \tag{51}$$

Now Applying finite sine Fourier transform, we get

$$\frac{sL_1 B\bar{\Psi}_{FT}(k,s)}{(s+L_2)} = \frac{P\left(1-(-1)^k\right)}{s\chi_k} + \frac{\chi_k}{s} - \chi_k^2\bar{\Psi}_{FT}(k,s), \tag{52}$$

or equivalently:

$$\bar{\Psi}_{FT}(k,s) = \left(\frac{P\left(1-(-1)^k\right)+\chi_k^2}{\chi_k\left(BL_1+\chi_k^2\right)}\right) \times \left(\frac{(s+L_2)}{s\,(s+L_{10})}\right), \tag{53}$$

where $B = \varphi_0\varphi_1 \mathrm{Re}$, and $L_{10} = \frac{H_2\delta_s^2}{B_1L_1+\delta_s^2}$.

Apart equation (53) w.r.t. s, we get:

$$\bar{\Psi}_{FT}(k,s) = \left(\frac{P\left(1-(-1)^k\right)+\chi_k^2}{\chi_k\left(BL_1+\chi_k^2\right)}\right) \times \left(\frac{L_2}{sL_{10}} + \frac{L_{11}}{s+L_{10}}\right). \tag{54}$$

Inverting the Laplace transform, we get the following form:

$$\Psi_{FT}(k,\tau) = \left(\frac{P\left(1-(-1)^k\right)+\chi_k^2}{\chi_k\left(BL_1+\chi_k^2\right)}\right) \times \left(\frac{\frac{L_2}{L_{10}}+}{L_{11}\exp(-L_{10}\tau)}\right). \tag{55}$$

By partial fraction of equation (55), we get:

$$\Psi_{FT}(k,\tau) = \frac{1-(-1)^k}{\chi_k} + \frac{(-1)^k}{\chi_k} + \frac{P\left(1-(-1)^k\right)}{\chi_k^3} + \kappa_k L_{11}\exp(-L_{10}\tau), \tag{56}$$

$$\text{where } L_{11} = 1 - \frac{L_2}{L_{10}} \text{ and } \kappa_k = \frac{P\left(1-(-1)^k\right)+\chi_k^2}{\chi_k\left(BL_1+\chi_k^2\right)}. \tag{57}$$

Inverting finite fine-Fourier transform, we get the final results takes the shape:

$$\Psi(\xi,\tau) = 1 - \frac{\xi}{\ell} - \frac{P\xi^2}{2} + \frac{2}{\ell}\sum_{k=1}^{\infty}\left[\kappa_k L_{11}\exp(-L_{10}\tau)\right]\sin(\chi_k\xi). \tag{58}$$

B. CSNF MODEL IN THE ABSENCE OF EXTERNAL PRESSURE GRADIENT

By taking ($P = 0$) in equation (19), we get the dimensionless form of present problem in the following form:

$${}^{CF}D_{\tau}^{\alpha} M\Psi(\xi,\tau) = \frac{\partial^2 \Psi(\xi,\tau)}{\partial \xi^2} - \lambda\frac{\partial^4 \Psi(\xi,\tau)}{\partial \xi^4} + A_0\Theta(\xi,\tau) + A_1\Phi(\xi,\tau). \tag{59}$$

By applying LT and finite sine Fourier transform, we get:

$$\begin{aligned}\bar{\Psi}_{FT}(k,s) &= \left(\frac{\chi_k^2+\lambda\chi_k^4}{s\chi_k\left(\chi_k^2+\lambda\chi_k^4\right)}\right) + \left(\frac{\chi_k^2+\lambda\chi_k^4}{\chi_k\left(ML_1+\chi_k^2+\lambda\chi_k^4\right)(s+L_9)}\right) \\ &- \left(\frac{\chi_k^2+\lambda\chi_k^4}{\chi_k\left(\chi_k^2+\lambda\chi_k^4\right)(s+L_9)}\right) \\ &+ \frac{A_0L_4}{\left(ML_1+\chi_k^2+\lambda\chi_k^4\right)}\left(\frac{L_2}{L_3 s} + \frac{2L_5}{s+L_3} + \frac{2L_5(L_2-L_3)}{(s+L_3)^2}\right) \\ &+ \frac{A_1L_7}{\left(ML_1+\chi_k^2+\lambda\chi_k^4\right)}\left(\frac{L_2}{L_6 s} + \frac{2L_8}{s+L_6} + \frac{2L_8(L_2-L_6)}{(s+L_6)^2}\right).\end{aligned} \tag{60}$$

Inverting the integral transforms, we get the following form:

$$\begin{aligned}\Psi(\xi,\tau) &= 1 - \frac{\xi}{\ell} + \frac{2}{\ell}\sum_{k=1}^{\infty}\left[(\alpha_{1k}-\beta_{1k})\exp(-L_9\tau)\right]\sin(\chi_k\xi) \\ &+ \frac{2}{\ell}\sum_{k=1}^{\infty}\left[\delta_{1k}A_0\exp(-L_3\tau)\right]\sin(\chi_k\xi) \\ &+ \frac{2}{\ell}\sum_{k=1}^{\infty}\left[\gamma_{1k}A_1\exp(-L_6\tau)\right]\sin(\chi_k\xi),\end{aligned} \tag{61}$$

where

$$M = \varphi_0\varphi_1 Re,$$

$$\alpha_{1k} = \left(\frac{\delta_k^2+\lambda\chi_k^4}{\chi_k\left(ML_1+\chi_k^2+\lambda\chi_k^4\right)}\right),$$

$$\beta_{1k} = \left(\frac{\chi_k^2+\lambda\chi_k^4}{\chi_k\left(\chi_k^2+\lambda\chi_k^4\right)}\right),$$

$$\delta_{1k} = \left(\frac{L_2}{L_3} + 2L_5 + 2L_5(L_2-L_3)\tau\right)\frac{L_4}{\left(ML_1+\chi_k^2+\lambda\chi_k^4\right)},$$

$$\gamma_{1k} = \left(\frac{L_2}{L_6} + 2L_8 + 2L_8(L_2-L_6)\tau\right)\frac{L_7}{\left(ML_1+\chi_k^2+\lambda\chi_k^4\right)}.$$

V. LIMITING CASES

Our obtained general solutions have been reduced to the already published works by substituting favorable limits of different parameters.

A. CLASSICAL CSNF MODEL

The solutions obtained in equation (45) is for a fractional model. To achieve the solutions for classical model for CSF, taking limit $\alpha \to 1$, $Gr \to 0$ and $Gm \to 0$, we will get:

$$\begin{aligned}
&\lim_{\alpha\to 1}{}^{CF}D_\tau^\alpha \Psi(\xi,\tau)\\
&= \lim_{\alpha\to 1}\left[L^{-1}\left\{L\,{}^{CF}D_\tau^\alpha \Psi(\xi,\tau)\right\}\right]\\
&= \lim_{\alpha\to 1}\left[L^{-1}\left\{\frac{s\bar{\Psi}(\xi,s)-\Psi(\xi,0)}{s(1-\alpha)+\alpha}\right\}\right]\\
&= L^{-1}\left[\lim_{\alpha\to 1}\left\{\frac{s\bar{\Psi}(\xi,s)-\Psi(\xi,0)}{s(1-\alpha)+\alpha}\right\}\right]\\
&= L^{-1}\left[s\bar{\Psi}(\xi,s)-\Psi(\xi,0)\right]\\
&= \Psi'(\xi,\tau)\\
&\Psi(\xi,\tau)\\
&= \begin{pmatrix} 1-P-\left(\frac{1}{\ell}-\frac{P\ell}{2}\right)\xi \\ -\frac{P}{2}\xi^2+P\left(\frac{\cosh\left(\frac{\ell}{2}-\xi\right)}{\cosh\left(\frac{\ell}{2}\right)}\right)\end{pmatrix}\\
&\quad+\frac{2}{h}\sum_{k=1}^{\infty}\left[\left(\frac{P\left(1-(-1)^k\right)}{\chi_k^3\left(1+\chi_k^2\right)}+\frac{1}{\chi_k}\right)\exp\left(-\frac{\chi_k^2+\lambda\chi_k^4}{\mathrm{Re}}\right)\right]\\
&\quad\times\sin(\chi_k\xi)\,. \qquad (62)
\end{aligned}$$

The results achieved in equation (62) is the same as results of Akhtar and Shah [65], hence this validates the correctness of the present study.

B. CSNF MODEL WITHOUT THERMAL AND CONCENTRATION

By taking limit $Gr \to 0$ and $Gm \to 0$ in the obtained solution i.e. equation (45), we get,

$$\begin{aligned}
&\Psi(\xi,\tau)\\
&= \begin{pmatrix} 1-P-\left(\frac{1}{\ell}-\frac{P\ell}{2}\right)\xi-\frac{P}{2}\xi^2 \\ +P\left(\frac{\cosh\left(\frac{\ell}{2}-\xi\right)}{\mathrm{osh}\left(\frac{\ell}{2}\right)}\right)\end{pmatrix}\\
&\quad+\frac{2}{\ell}\sum_{k=1}^{\infty}\left[\begin{pmatrix}\frac{P\left(1-(-1)^k\right)+\chi_k^2+\lambda\chi_k^4}{\chi_k\left(\psi_1 L_1+\chi_k^2+\lambda\chi_k^4\right)} \\ -\frac{P\left(1-(-1)^k\right)+\chi_k^2+\lambda\chi_k^4}{\chi_k\left(\chi_k^2+\lambda\chi_k^4\right)}\end{pmatrix}e^{-L_9\tau}\right]\sin(\chi_k\xi)\,. \qquad (63)
\end{aligned}$$

Equation (63) is the obtained solution by Arif *et al.* [33]. Hence it validates our solutions and it verify our obtained solutions of the present problem.

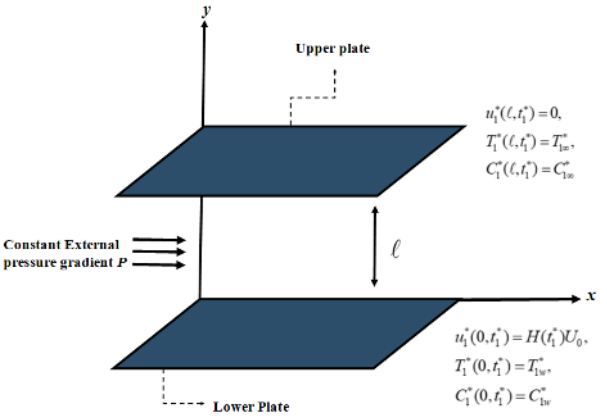

FIGURE 1. Geometry of the problem.

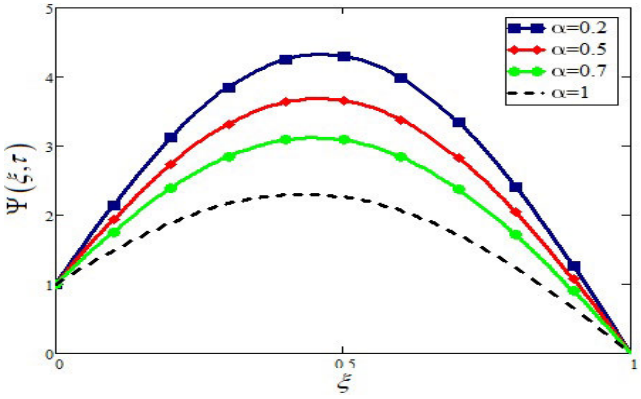

FIGURE 2. α impact on CSNF velocity distribution when $P = 2$, $Gr = 1.5$, $Gm = 1.5$, Re $= 0.5$, Pr $= 1000$, $\tau = 2$, $\phi = 0.01$, $Sc = 2$ and $\lambda = 50$.

TABLE 1. Thermo-physical properties of EO and MoS_2 [54]–[56].

Material	ρ Kgm^{-3}	c_p $JKg^{-1}K^{-1}$	k $wm^{-1}K^{-1}$	$\beta\times10^{-5}$ K^{-1}
Engine Oil	863	2048	0.1404	0.00007
MoS_2	5.06×10^3	397.21	904.4	2.8424

VI. NUSSELT NUMBER, SHERWOOD NUMBER AND SKIN FRICTION

A. NUSSELT NUMBER

The Mathematical expression for the Nusselt number of CSNF is given by:

$$Nu = -\frac{k_{nf}}{k_f}\left.\frac{\partial\Theta}{\partial\xi}\right|_{\xi=0}. \qquad (64)$$

B. SHERWOOD NUMBER

The mathematical expression for the Sherwood number of CSNF is given by:

$$S_h = -D_{nf}\left.\frac{\partial\Phi}{\partial\xi}\right|_{\xi=0}. \qquad (65)$$

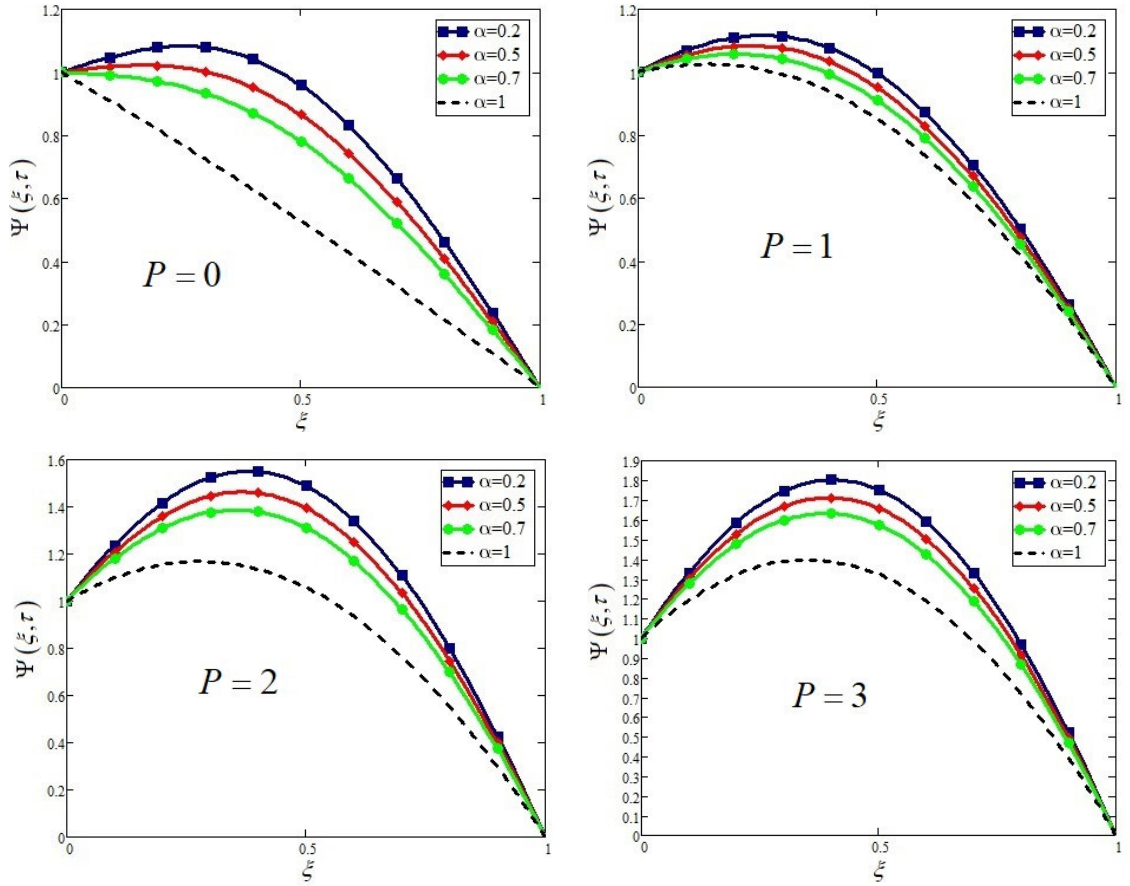

FIGURE 3. *P* impact on CSNF velocity distribution when $Gr = 1.5$, $Gm = 1.5$, $\mathrm{Re} = 0.5$, $\mathrm{Pr} = 1000$, $\tau = 2$, $\phi = 0.01$, $Sc = 2$ and $\lambda = 50$.

TABLE 2. The skin friction of EO based-MoS_2 CSNF at the lower plate.

P	Gr	Gm	Re	λ	τ	ϕ	Pr	Sc	α	C_f^{α}	$C_f^{classical}$
2	1.5	1.5	0.5	50	2	0.01	1000	2	0.5	**2.349**	**1.221**
3	1.5	1.5	0.5	50	2	0.01	1000	2	0.5	**3.422**	**2.294**
2	**2.5**	1.5	0.5	50	2	0.01	1000	2	0.5	**2.714**	**1.228**
2	1.5	**2.5**	0.5	50	2	0.01	1000	2	0.5	**2.803**	**2.355**
2	1.5	1.5	**0.6**	50	2	0.01	1000	2	0.5	**2.330**	**1.208**
2	1.5	1.5	0.5	**60**	2	0.01	1000	2	0.5	**2.144**	**1.204**
2	1.5	1.5	0.5	50	**2.5**	0.01	1000	2	0.5	**2.907**	**1.274**
2	1.5	1.5	0.5	50	2	**0.03**	1000	2	0.5	**4.848**	**1.469**
2	1.5	1.5	0.5	50	2	0.01	**1080**	2	0.5	**2.349**	**1.221**
2	1.5	1.5	0.5	50	2	0.01	1000	**3**	0.5	**2.304**	**1.194**
2	1.5	1.5	0.5	50	2	0.01	1000	2	**0.6**	**2.218**	**1.221**

C. SKIN FRICTION

The mathematical expression of skin friction for CSNF is given as

$$Sf(\xi,\tau) = \frac{1}{(1-\phi)^{2.5}}\left(\frac{\partial\Psi}{\partial\xi} - \frac{\partial^3\Psi}{\partial\xi^3}\right). \tag{66}$$

As in the given problem, we have a bounded domain in which the flow is between two infinite plates. Therefore the skin friction at the lower and upper plates are given by:

$$Sf_{lp}(0,\tau) = \frac{1}{(1-\phi)^{2.5}}\left(\frac{\partial\Psi}{\partial\xi} - \frac{\partial^3\Psi}{\partial\xi^3}\right)_{\xi=0}, \tag{67}$$

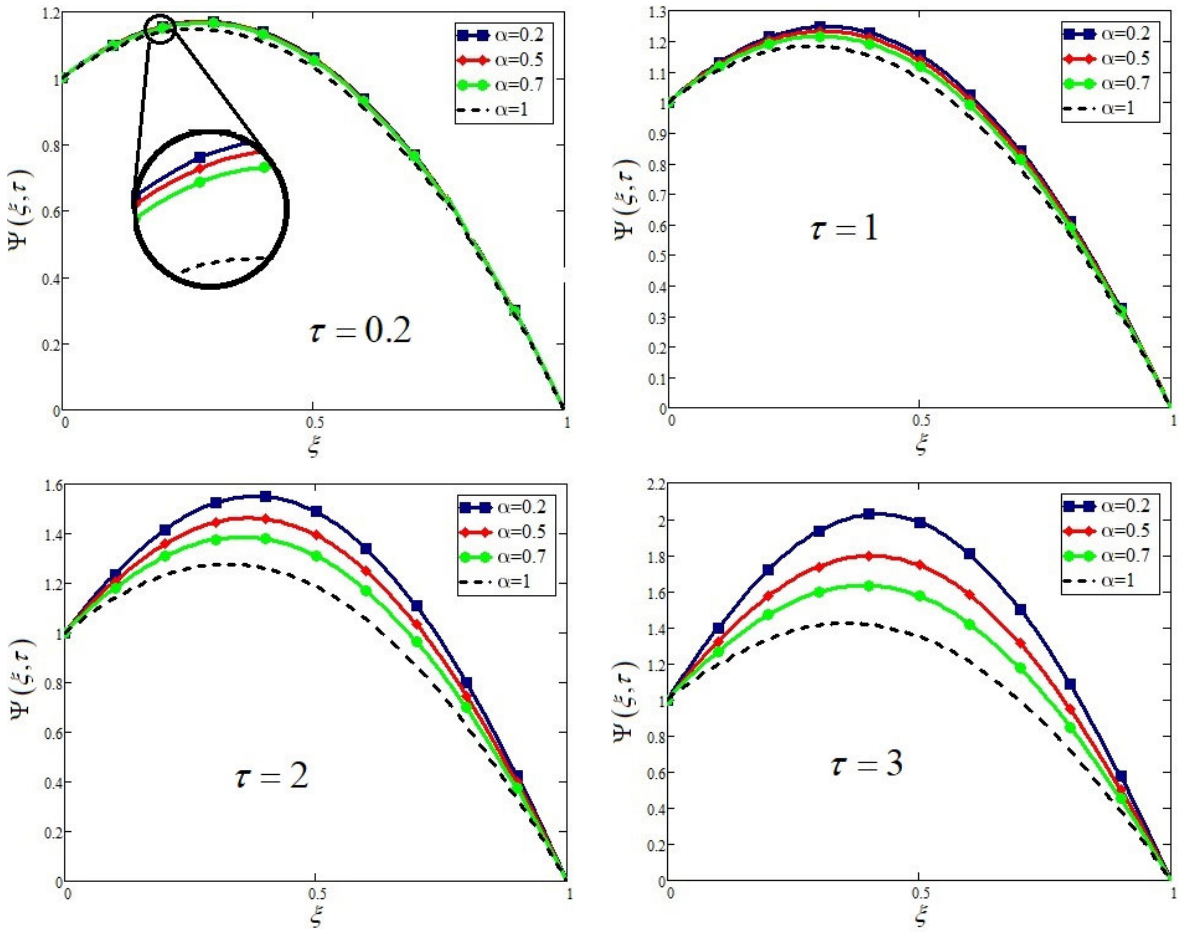

FIGURE 4. τ impact on CSNF velocity distribution when $P = 2$, $Gr = 1.5$, $Gm = 1.5$, Pr = 1000, Re = 0.5, $\phi = 0.01$, $Sc = 2$ and $\lambda = 50$.

TABLE 3. The skin friction of EO based-MoS_2 CSNF at the upper plate.

P	Gr	Gm	Re	λ	τ	ϕ	Pr	Sc	α	C_f^{α}	$C_f^{classical}$
2	1.5	1.5	0.5	50	2	0.01	1000	2	0.5	**1.051**	**2.110**
3	1.5	1.5	0.5	50	2	0.01	1000	2	0.5	**2.124**	**3.183**
2	**2.5**	1.5	0.5	50	2	0.01	1000	2	0.5	**0.709**	**2.104**
2	1.5	**2.5**	0.5	50	2	0.01	1000	2	0.5	**0.632**	**2.061**
2	1.5	1.5	**0.6**	50	2	0.01	1000	2	0.5	**1.070**	**2.121**
2	1.5	1.5	0.5	**60**	2	0.01	1000	2	0.5	**1.241**	**2.124**
2	1.5	1.5	0.5	50	**2.5**	0.01	1000	2	0.5	**0.535**	**2.067**
2	1.5	1.5	0.5	50	2	**0.03**	1000	2	0.5	**1.102**	**2.070**
2	1.5	1.5	0.5	50	2	0.01	**1080**	2	0.5	**1.051**	**2.110**
2	1.5	1.5	0.5	50	2	0.01	1000	**3**	0.5	**1.095**	**2.133**
2	1.5	1.5	0.5	50	2	0.01	1000	2	**0.6**	**1.75**	**2.110**

$$Sf_{up}(1,\tau) = \frac{1}{(1-\phi)^{2.5}}\left(\frac{\partial\Psi}{\partial\xi} - \frac{\partial^3\Psi}{\partial\xi^3}\right)_{\xi=1}, \quad (68)$$

where Sf_{lp} and Sf_{up} denotes the skin friction at lower and upper plates respectively.

VII. RESULTS AND DISCUSSION

In the present study, we derived the exact solutions for the generalized couette flow of EO based-MoS_2 CSNF with the joint effect of heat and mass transfer. The closed form

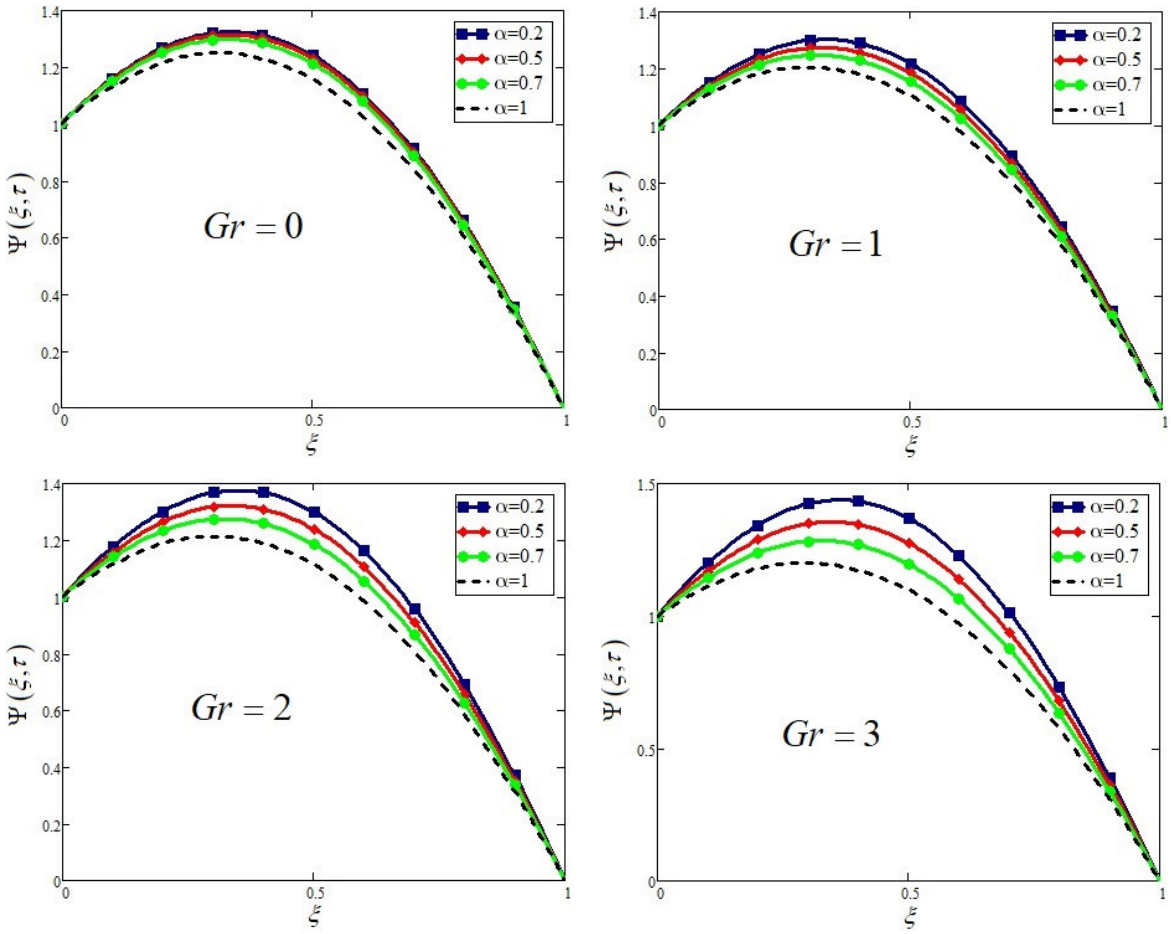

FIGURE 5. *Gr* impact on CSNF velocity distribution when $P = 2$, $Gm = 1.5$, $\mathrm{Pr} = 1000$, $\mathrm{Re} = 0.5$, $\tau = 2$, $\phi = 0.01$, $Sc = 2$and$\lambda = 50$.

TABLE 4. Nusselt number for EO based-MoS_2 CSNF.

α	Pr	τ	ϕ	*Nu*	Heat Transfer Enhancement
0.5	1000	2	**0.00**	**1.009**	**--**
0.5	1000	2	**0.01**	**1.04**	**3.07%**
0.5	1000	2	**0.02**	**1.071**	**6.15%**
0.5	1000	2	**0.03**	**1.102**	**9.22%**
0.5	1000	2	**0.04**	**1.134**	**12.38%**

solutions have been obtained by using the combine applications of Fourier and Laplace transforms. Generalized couette flow of CSNF have been considered by utilizing the most recently proposed definition of fractional derivative namely Caputo-Fabrizio fractional derivative. The graphical results of fractional order derivative are compared with the classical derivative. The obtained results are reduced to the simple classical CSNF and Newtonian viscous fluid in limiting sense. The comparison of the CSNF velocity is compared graphically with the classical CSNF and Newtonian viscous fluid velocity. Physical geometry of the present problem is shown in figure 1. The obtained solutions for velocity distribution are portrayed in figure 2 to figure 15, results for temperature distribution are shown in figure 16 to figure 18, the results for concentration distribution are displayed in figure 19 to figure 21 and skin friction, Nusselt number and Sherwood number is portrayed in figure 22 to figure 24 respectively. The thermophysical properties of nanoparticles are shown in table 1. The numerical values for skin friction at lower and upper plate are shown in table 2 and table 3 respectively.

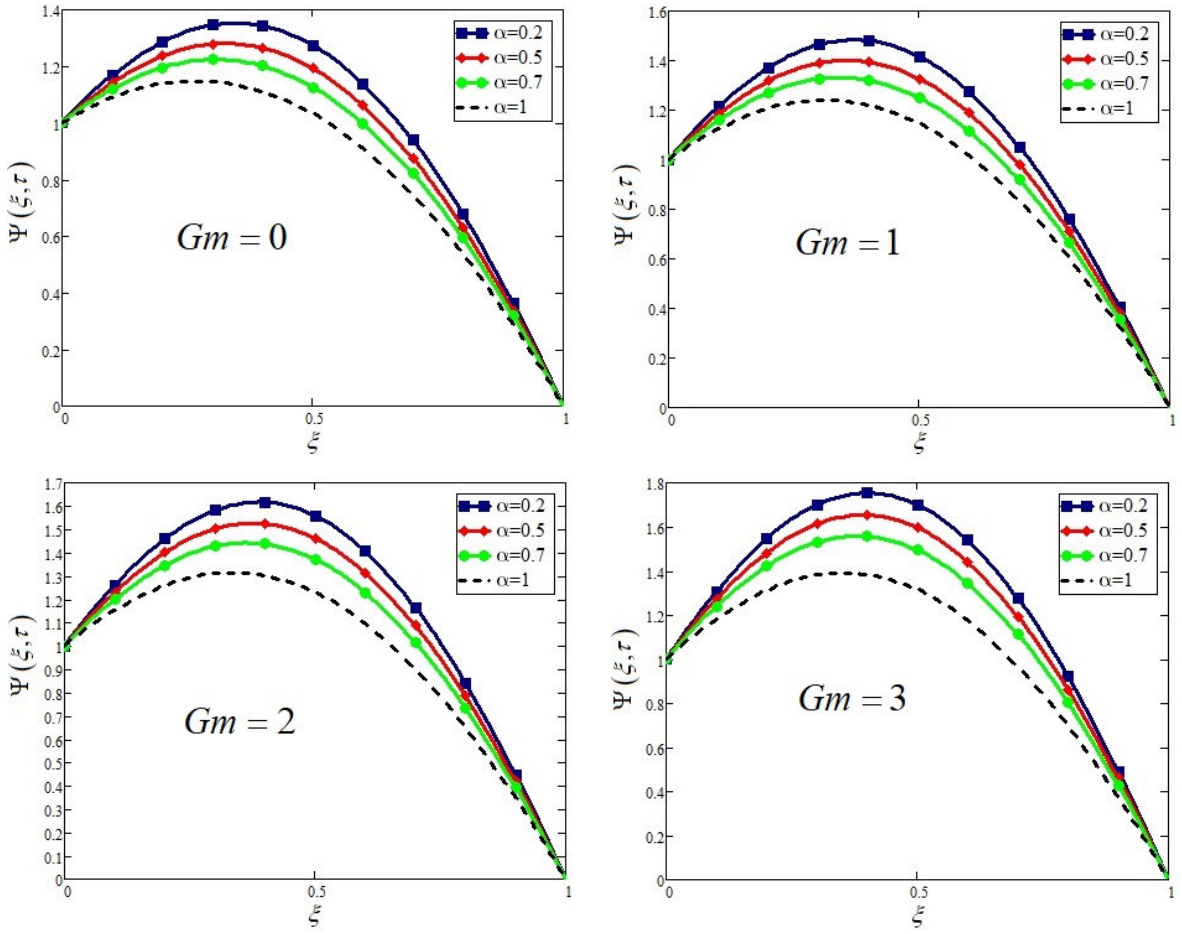

FIGURE 6. *Gm* impact on CSNF velocity distribution when $P = 2$, $Gr = 1.5$, $\mathrm{Pr} = 1000$, $\mathrm{Re} = 0.5$, $\tau = 2$, $\phi = 0.01$, $Sc = 2$ and $\lambda = 50$.

TABLE 5. Sherwood number for EO based-MoS_2 CSNF.

α	Sc	τ	ϕ	S_h	Decrease in Mass Distribution
0.5	2	2	**0.00**	**0.607**	**--**
0.5	2	2	**0.01**	**0.603**	**0.65%**
0.5	2	2	**0.02**	**0.600**	**1.15%**
0.5	2	2	**0.03**	**0.597**	**1.65%**
0.5	2	2	**0.04**	**0.594**	**2.14%**

The numerical values for Nusselt and Sherwood numbers are shown in table 4 and table 5 respectively.

As in the present paper, we are interested to derive the solutions of CF derivatives. The influence of α on the velocity distribution is displayed in figure 2. From the figure, we observed that increasing α results to reduce the CSNF velocity. In order to observe the differences clearly, all the figures are compared for integer order $\alpha = 1$ and fractional order $0 < \alpha < 1$ which provide us many solutions as compare to $\alpha = 1$. From all these figures, it can be noticed that the classical velocity is less in magnitude than that of fractional velocity. For the case, $\alpha = 1$, the obtained solutions reduced to the solutions of Akhtar and Shah [65] which verify our obtained results. Figure 3 demonstrates the influence of P on the CSNF velocity. By increasing numerical value of P from $P = 2$ to $P = 3$, the CSNF velocity increases. As it is obvious that P increases the fluid motion in a channel. In figure 4, the behavior of CSNF velocity has been shown

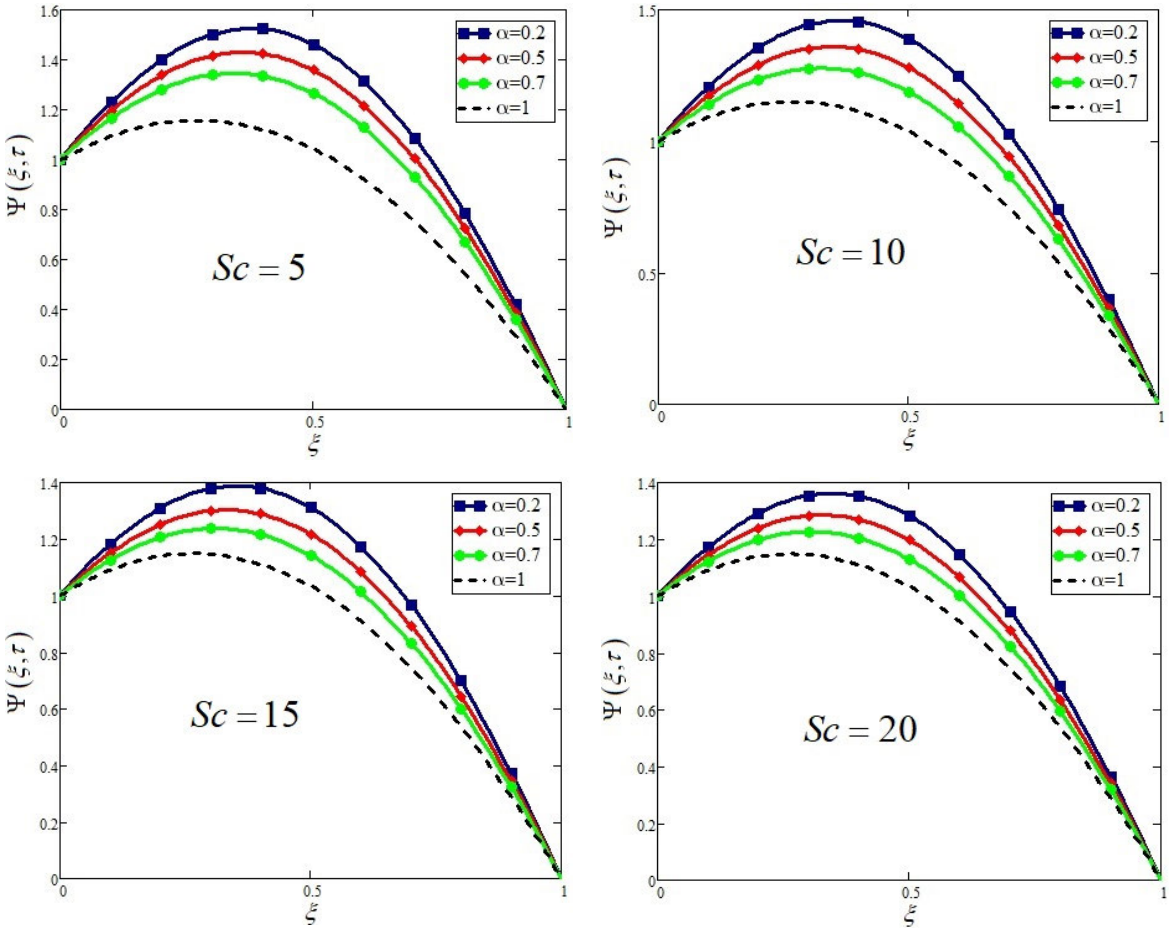

FIGURE 7. *Sc* impact on CSNF velocity distribution when $P = 2$, $Gr = 1.5$, $Gm = 1.5$, $\mathrm{Pr} = 1000$, $\mathrm{Re} = 0.5$, $\tau = 2$, $\phi = 0.01$ and $\lambda = 50$.

for different values of τ. From the figure, it is clearly noticed that for small as well as for large values of τ, there is an increase in fractional as will as classical velocity of CSNF. As in the given problem, we assume an unsteady flow of CSNF, so the velocity of CSNF is dependent of τ. The influence of *Gr* and *Gm* has been presented in figure 5 and figure 6 respectively. It is observed that by increasing the numerical values of both *Gr* and *Gm* accelerates the velocity of CSNF. Physically, it is true because increasing values of *Gr* and *Gm*, results to increase the buoyancy forces that decreases the fluid viscosity and increases the CSNF velocity. Figure 7 displays the velocity profile of CSNF for distinct values of *Sc* which produces a decrease in the velocity of CSNF. It is true because *Sc* is the ratio of viscous forces to mass diffusion. By increasing numerical value of *Sc* results a rise in the viscous forces and decrease in mass diffusion which results the reduction of CSNF velocity. The impact of ϕ on velocity profile has been shown in figure 8. By increasing the numerical value of ϕ (from 0.01 to 0.04) decreases the velocity profile. The cause of decreasing velocity is that by increasing ϕ, the fluid viscosity increases and as a result, the retardation of velocity occurs. Figure 9 demonstrates the influence of λ on the velocity distribution. By increasing value of λ, decreases the CSNF velocity. The fact behind this is that, as we have chosen molybdenum disulphide nanoparticles dispersed in EO. Generally, when we disperse some additives in the fluid, the forces existing in the fluid opposes the forces caused by additives. The couples force generated by this opposite force and a couple stress is generated in the fluid motion. The influence of Pr and Re on the velocity distribution is presented in figure 10 and figure 11 respectively. A decrease in the velocity profile can be seen by increasing value of Pr and Re. As by increasing Pr, fluids possess greater viscosities and this results to decrease CSNF velocity. Similarly, as Re is the ratio between inertial and viscous forces. By increasing Re, it means that turbulence is generated in the fluid which increases viscous forces and results to reduce the CSNF velocity. In the present study, we have discussed two special cases and two limiting cases of the obtained results. The first special case is to compare the velocity of CSNF with and without *P* and the second case is to compare the results of CSNF velocity with classical Newtonian viscous fluid velocity. Similarly, the first limiting case is to reduce the obtained results to the results obtained by Akhtar and

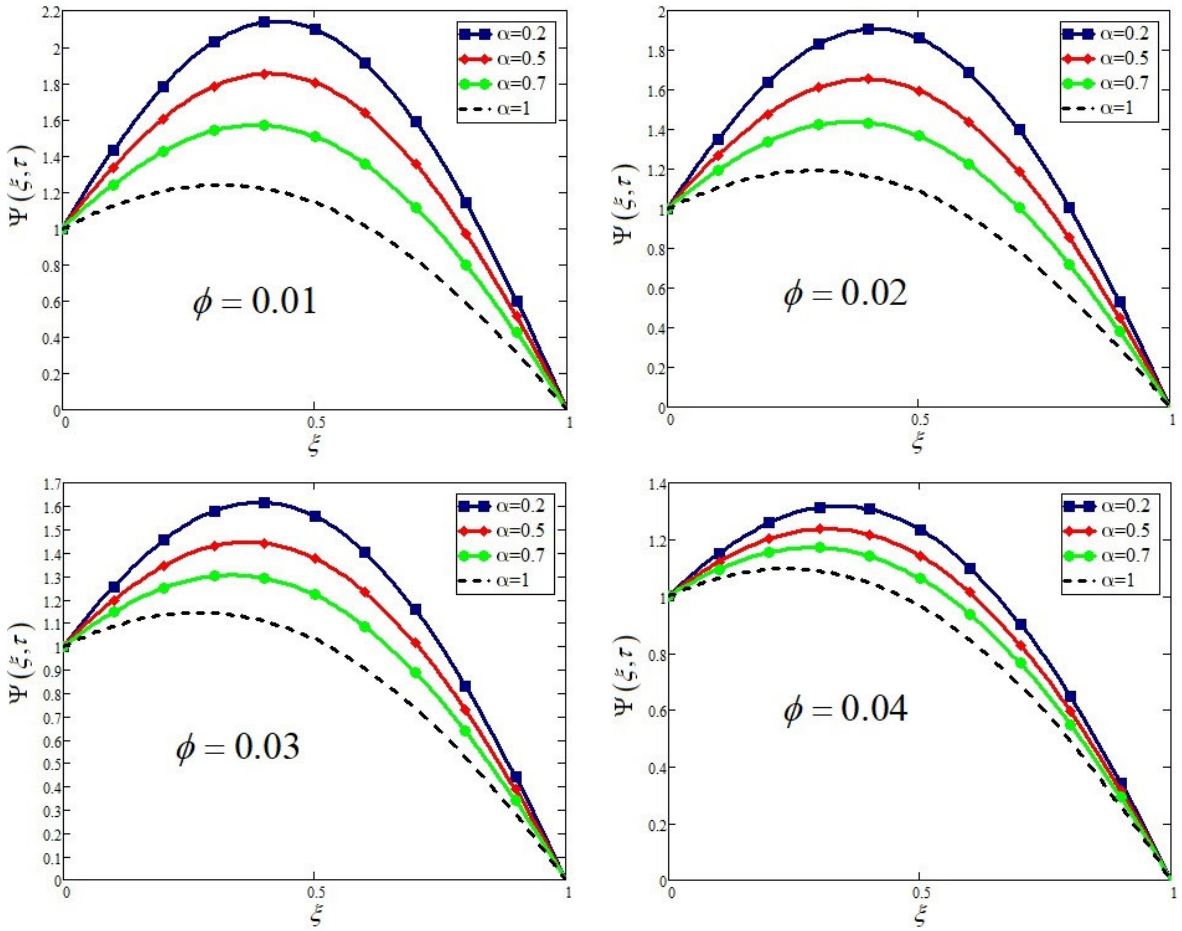

FIGURE 8. ϕ impact on CSNF velocity distribution when $P = 2$, $Gr = 1.5$, $Gm = 1.5$, Pr = 1000, Re = 0.5, $\tau = 2$, $Sc = 2$ and $\lambda = 50$.

Shah [65] and the second limiting case is to reduce the present reults to Arif *et al.* [33]. It is worth noting that the limiting cases of our obtained solutions are in good argument with the published work. The comparison of the velocity with and without pressure gradient P is displayed in figure 12. The role of P is to enhance the fluid velocity. It can be seen in the figure that P accelerates the motion of CSNF. In figure 13 the comparison of Newtonian viscous fluid velocity and CSNF velocity is displayed. It can be seen that the velocity of Newtonian viscous fluid is higher than CSNF velocity. The fact behind this is that, as in figure 10, we have already seen the role of λ on the CSNF velocity. As increasing value of λ results the retardation of the CSNF velocity. In Newtonian viscous fluid, we have taken $\lambda = 0$. Therefore the Newtonian viscous fluid velocity is much more as compared to CSNF velocity. In figure 14, the obtained solutions are compared to the solutions of Akhtar and Shah [65]. From the figure we have noticed that by taking $\alpha = 1$, $Gr = 0$ and $Gm = 0$, our solutions reduced to the solutions of Akhtar and Shah [65] and overlap our results with the already published results of Akhtar and Shah [65]. The comparison of present results with the published results of Arif *et al.* [33] are portrayed in figure 15. From the figure, we have seen that our results overlapped with the results of Arif *et al.* [33] in the absence of buoyancy effects i.e. by taking $Gr = 0$ and $Gm = 0$.

The influence of α on temperature distribution is displayed in figure 16. From the figure, fall in temperature distribution is noticed by increasing values of α for small values of time ($\tau = 0.2$) by keeping other values constant while opposite impact of α is noticed for large values of time ($\tau = 2$). In figure 17, the influence of ϕ on temperature distribution is displayed. We observed that heat transfer rate rises by increasing value of ϕ for small time ($\tau = 0.2$) as will as for the large time ($\tau = 2$). As by increasing ϕ, fluid viscosity increases which results to increase the freezing as will as boiling point of the fluid, and as a result, heat transfer rate enhances. Figure 18 presented the Pr impact on the temperature distribution. One can be notice that CSNF temperature profile declines for large values of Pr. The behavior of Pr is same for both small time ($\tau = 0.2$) as will as for the large time ($\tau = 2$) is same. As Pr has a direct variation with the viscosity. By increasing Pr, increases the viscous forces and as a result rise in temperature profile. The influence of α on

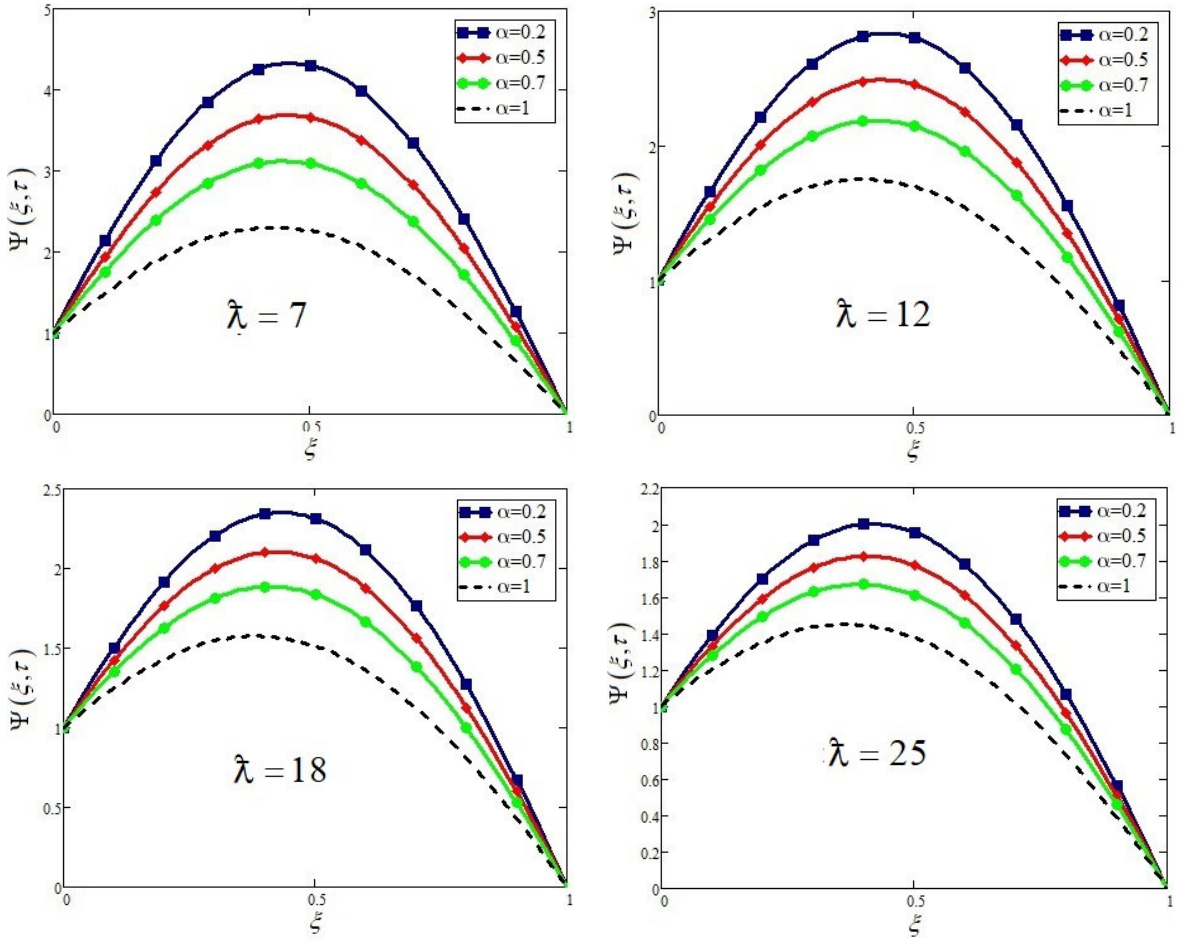

FIGURE 9. λ impact on CSNF velocity distribution when $P = 2$, $Gr = 1.5$, $Gm = 1.5$, Pr = 1000, Re = 0.5, $\tau = 2$, $\phi = 0.01$ and $Sc = 2$.

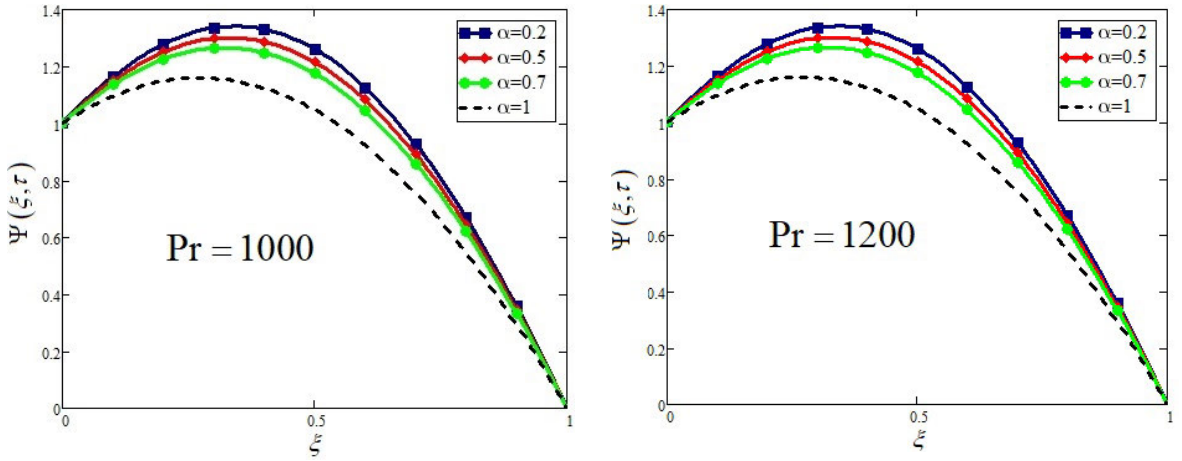

FIGURE 10. Pr impact on CSNF velocity distribution when $P = 2$, $Gr = 1.5$, $Gm = 1.5$, Re = 0.5, $\tau = 2$, $\phi = 0.01$, $Sc = 2$, $\alpha = 0.5$ and $\lambda = 50$.

concentration distribution is displayed in figure 19. From the figure, fall in concentration distribution is noticed by increasing values of α for small values of time ($\tau = 0.2$) by keeping other values constant while opposite impact of α is noticed for large values of time ($\tau = 2$). Figure 20 and figure 21 indicate the influence of ϕ and Sc on the concentration distribution

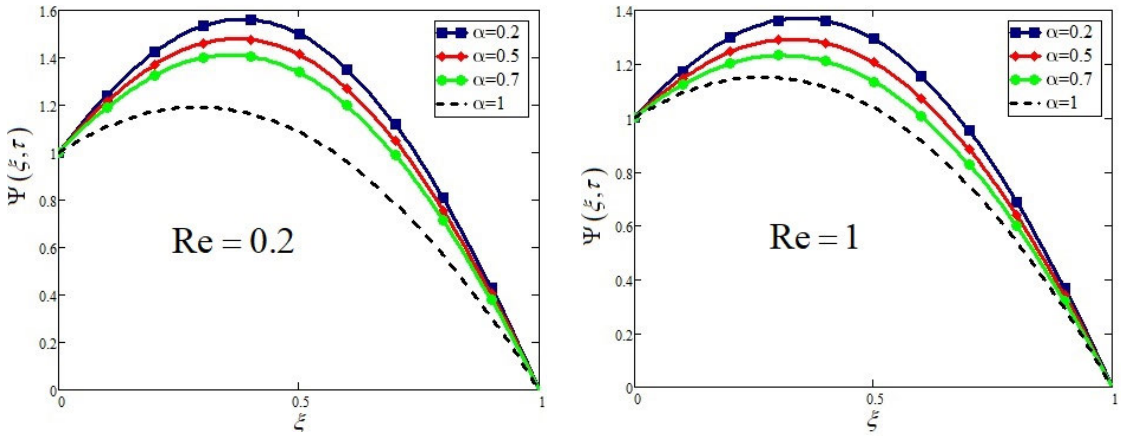

FIGURE 11. *Re* impact on CSNF velocity distribution when $P = 2$, $Gr = 1.5$, $Gm = 1.5$, Pr $= 1000$, $\tau = 2$, $\phi = 0.01$, $Sc = 2$ and $\lambda = 50$.

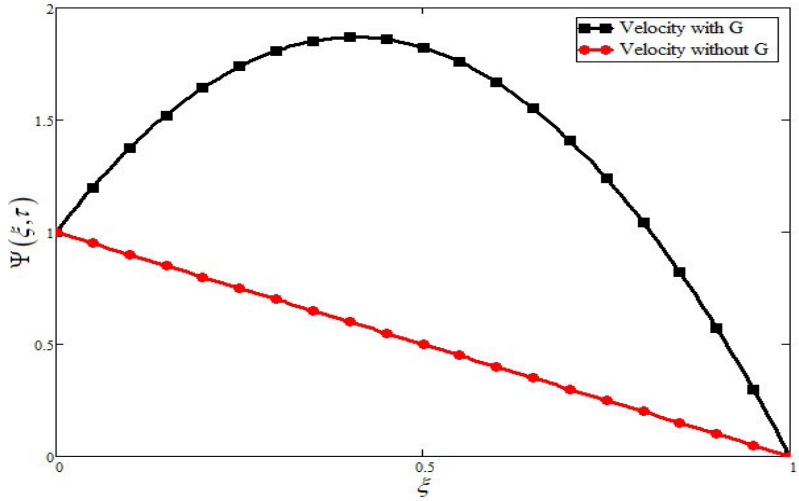

FIGURE 12. Comparison of CSNF velocities with $P = 0$ and $P > 0$ when $Gr = 1.5$, $Gm = 1.5$, Pr $= 1000$, Re $= 0.5$, $\tau = 2$, $\phi = 0.01$, $Sc = 2$, $\alpha = 0.5$ and $\lambda = 50$.

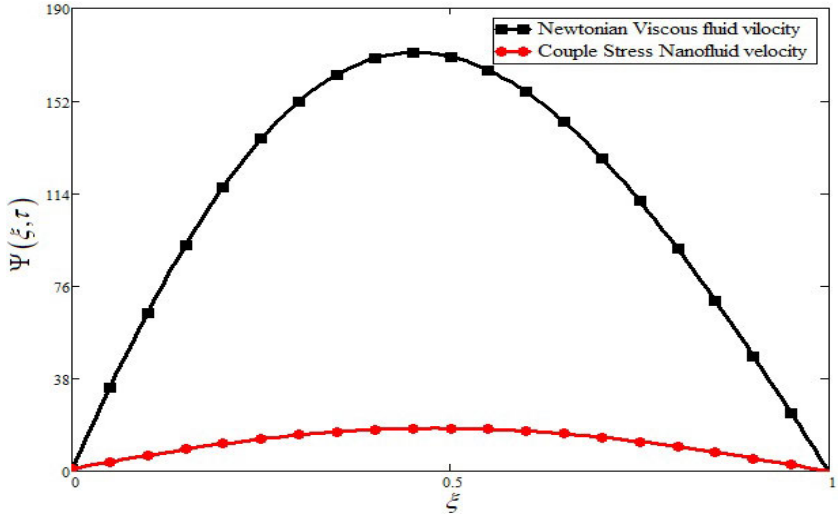

FIGURE 13. Comparison of Newtonian viscous fluid velocity with CSNF velocity when $G = 2$, $Gr = 1.5$, $Gm = 1.5$, Pr $= 1000$, Re $= 0.5$, $\tau = 2$, $\phi = 0.01$, $Sc = 2$ and $\alpha = 0.5$.

respectively. Fall in concentration profile can be seen clearly by increasing the value of ϕ and Sc for small time ($\tau = 0.2$) as will as for the large time ($\tau = 2$) The fact behind this is that by increasing ϕ, viscous forces of the fluid increases which slowdown the mass distribution in the fluid. Sc is the ratio of viscous forces to mass diffusion. By increasing

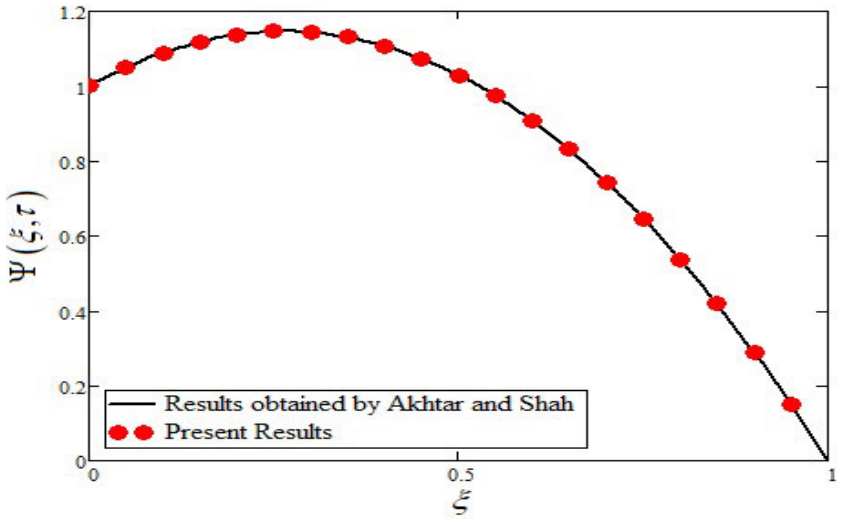

FIGURE 14. Comparison of obtained results with the results of Akhtar and Shah [65] when $P = 2$, $Gr = 0$, $Gm = 0$, Pr = 1000, Re = 0.5, $\tau = 2$, $\phi = 0.01$, $Sc = 2$, $\alpha = 1$ and $\lambda = 50$.

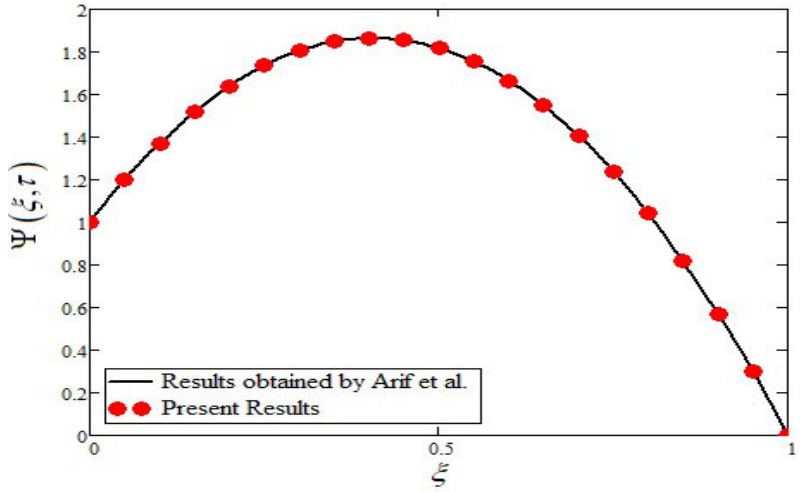

FIGURE 15. Comparison of obtained results with the results of Arif *et al.* [33] when $P = 2$, $Gr = 0$, $Gm = 0$, Pr = 1000, Re = 0.5, $\tau = 2$, $\phi = 0.01$, $Sc = 2$ and $\alpha = 0.5$.

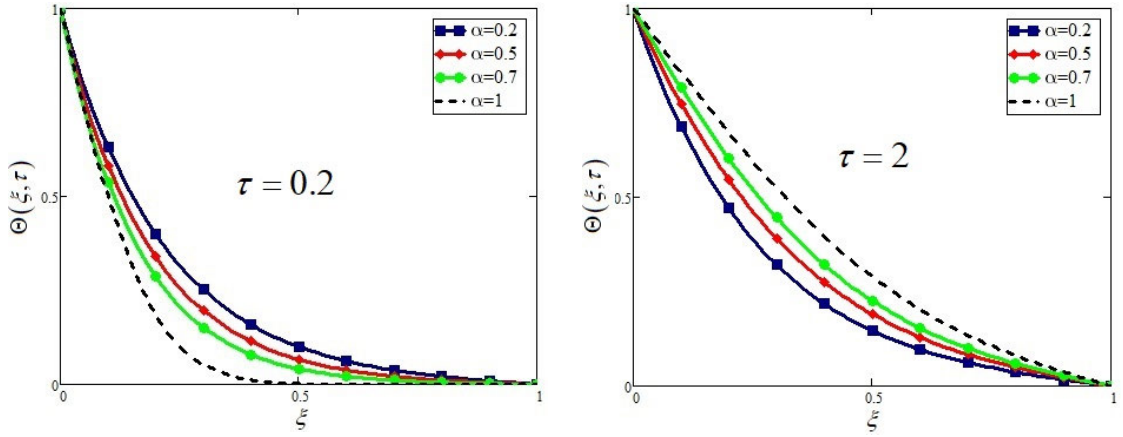

FIGURE 16. α impact on CSNF temperature distribution when Pr = 1000, $\phi = 0.01$.

numerical value of *Sc,* it means that we increases viscous forces or decreases mass diffusion, which results a decrease in concentration profile.

Figure 22 shows the skin friction variation at lower and upper plates for different values of ϕ. It is noticed from the figure that ϕ increases skin friction at lower as well as upper

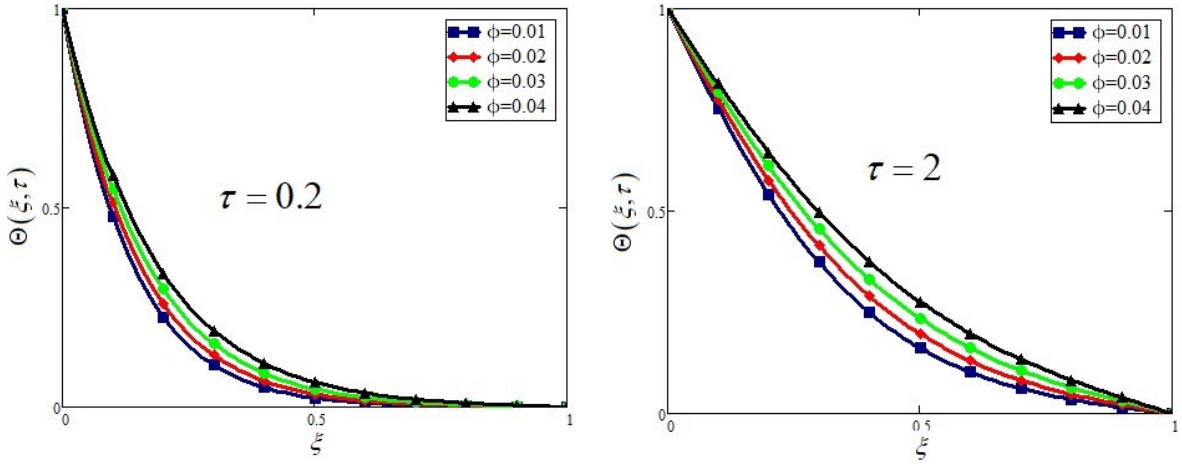

FIGURE 17. ϕ impact on CSNF temperature distribution when Pr = 1000, $\alpha = 0.5$.

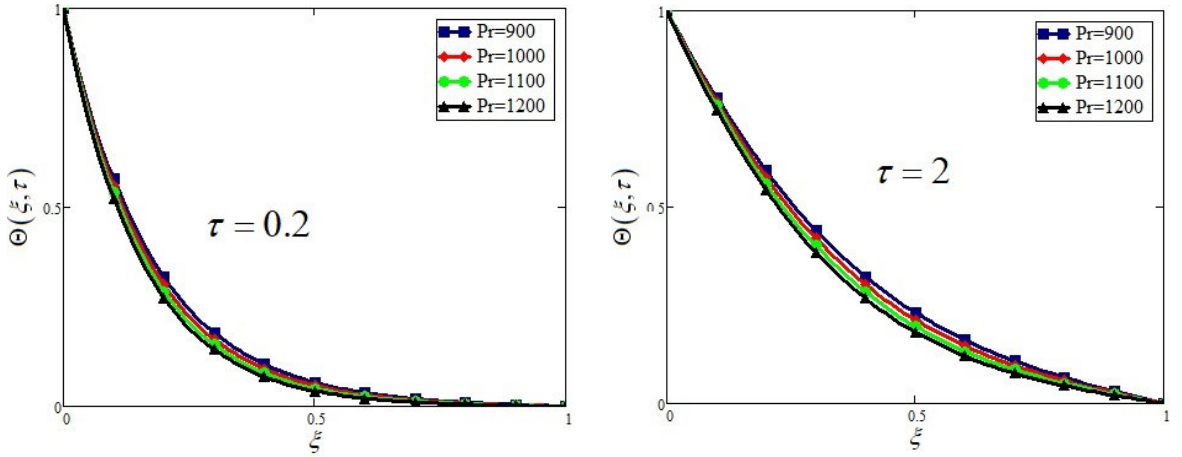

FIGURE 18. *Pr* impact on CSNF temperature distribution when $\phi = 0.01$, $\alpha = 0.5$.

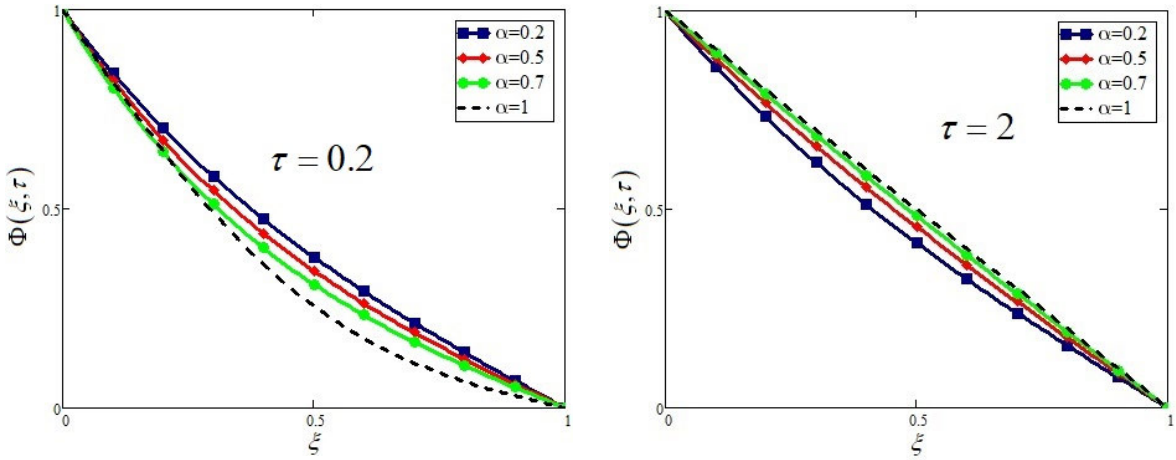

FIGURE 19. α impact on CSNF concentration distribution when $Sc = 2$, $\phi = 0.01$.

plate for large as well as for small time. Figure 23 depicts Nusselt number variation for different values of ϕ. It is clearly noticed that by icreasing value of ϕ form 0 to 0.04 increases the Nusselt number variation. Furthermore, the heat transfer rate increases upto 12.38% by adding MoS_2 nanoparticles in EO which shows that more heat can be absorbed from

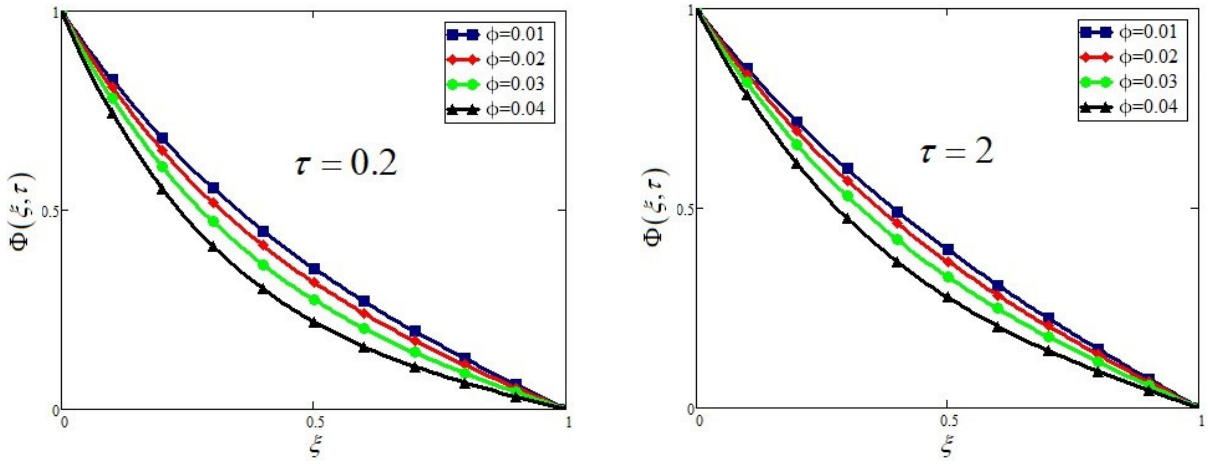

FIGURE 20. ϕ impact on CSNF concentration distribution when $Sc = 2, \alpha = 0.5$.

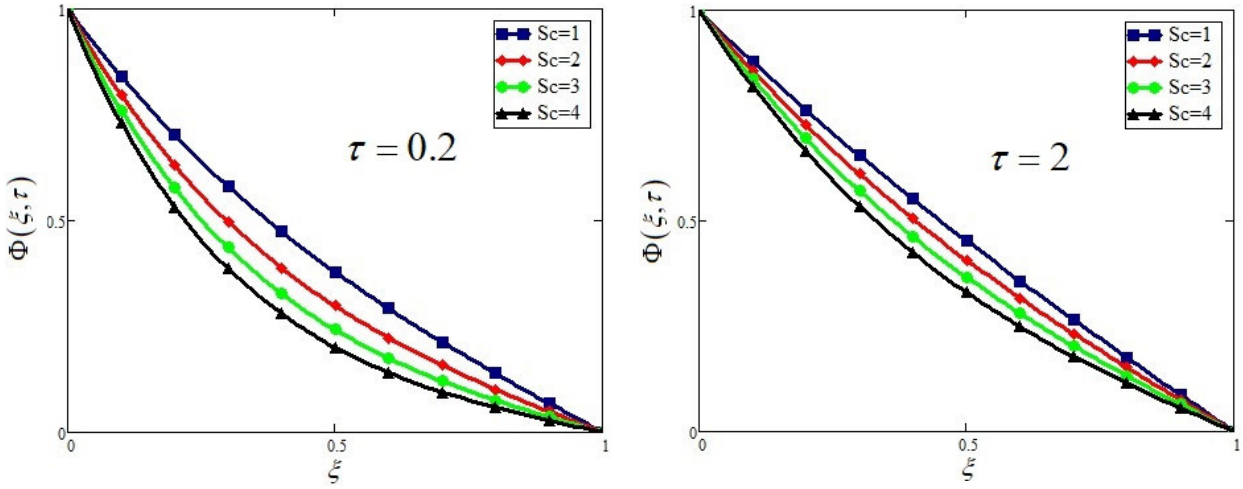

FIGURE 21. *Sc* impact on CSNF temperature distribution when $\phi = 0.01, \alpha = 0.5$.

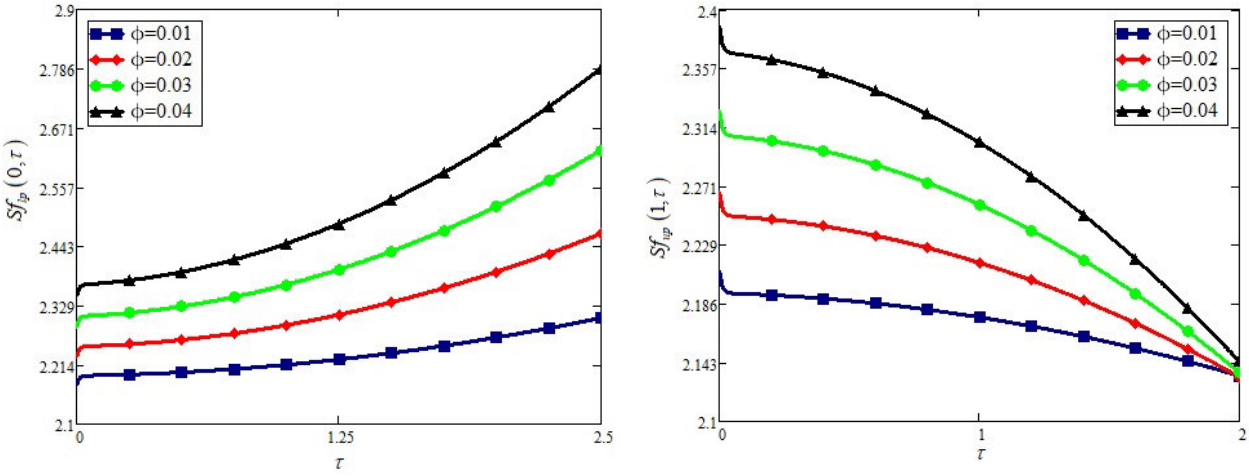

FIGURE 22. Variation in skin friction at lower plate for different values of ϕ when $P = 2$, $Gr = 1.5$, $Gm = 1.5$, $\Pr = 1000$, $\lambda = 50$, $\mathrm{Re} = 0.5$, $y = 0$, $Sc = 2$ and $\alpha = 0.5$

the engine and offcourse it will increase the life of engine. Figure 24 demonstrates the influence of ϕ on Sherwood number. From the figure, it can be clearly noticed that ϕ decreases the rate of mass transfer. It is worth noting that all these graphs depicts a strong argument with the numerical results which are tabulated in table 2 to table 5.

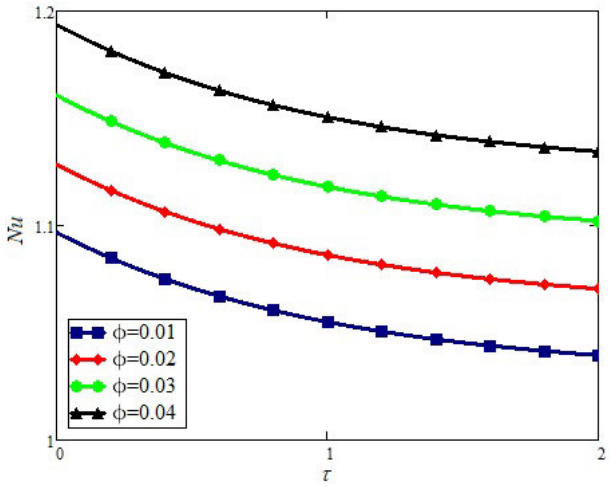

FIGURE 23. Variation in *Nu* for different values of ϕ when $\mathbf{Pr = 1000}$, $\alpha = 0.5$.

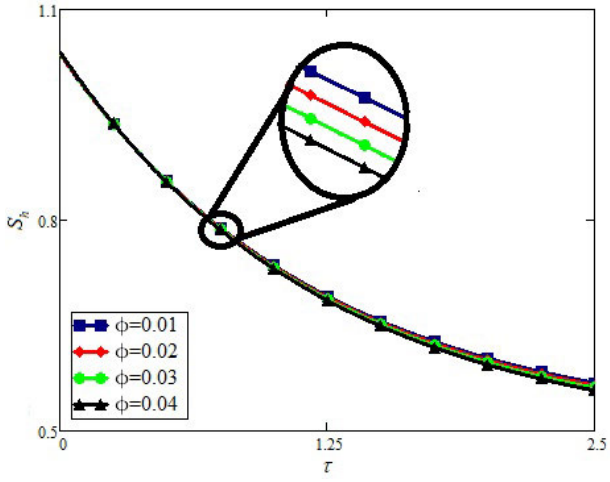

FIGURE 24. Variation in S_h for different values of ϕ when $Sc = 2$, $\alpha = 0.5$.

Table 2 and table 3 shows the variation in skin friction at lower as well as upper plate respectively. These tables show the results of skin friction for fractional as well as classical CSNF model. The influence of different embedded parameters on skin friction is also examined. Table 4 and table 5 depict the Nusselt and Sherwood numbers variations respectively for different values of ϕ. It is detected that heat transfer rate boosts up to 12.38% and mass distribution decreases up to 2.14% by increasing value of ϕ up to 0.04. As ϕ increases fluid viscosity which results increase the freezing and boiling points of the fluid.

VIII. CONCLUDING REMARKS

The aim of this study is to obtain the closed form solutions of CSNF between two parallel plates. The solutions are obtained for the recently most using fractional derivative namely Caputo-Fabrizio time fractional derivative. The obtained results are also displayed in the graphs. Engine oil is takes as base fluid and Molybednum disulphide is chosen as nanoparticles. From the present solutions, some special cases are recovered for the accuracy and validity of the solutions. The results of CF fractional derivatives are compared with the classical model through figures. The key points of the present study are listed below:

- From the graphical results, we noticed that the fractional CSNF model described more realistic feature of the velocity distribution better than the classical CSNF model.
- CSNF velocity is less than Newtonian viscous fluid velocity.
- Increase in the temperature profile and concentration profile is observed by increasing value of α for the small values of τ. Opposite effect of α is noticed for the large values of τ.
- Increasing temperature profile while decreasing concentration profile by increasing ϕ.
- Heat transfer enhances up to 12.38% by increasing as compared to regular engine oil.
- Mass transfer decreases up to 2.14% by increasing value of ϕ by 0.04.

REFERENCES

[1] V. K. Stokes, "Couple stresses in fluids," *Phys. Fluids*, vol. 9, no. 9, pp. 1709–1715, 1966.
[2] V. K. Stokes, *Theories of fluids with microstructure: An introduction*. Springer, 2012.
[3] V. Kumar and S. Kumar (2010), "On a couple-stress fluid heated from below in hydromagnetics," Applications and Applied Mathematics, vol. 5, no. 10, pp. 1529–1542.
[4] D. Tripathi, A. Yadav, and O. Anwar Bég, "Electro-osmotic flow of couple stress fluids in a micro-channel propagated by peristalsis," *Eur. Phys. J. Plus*, vol. 132, no. 4, pp. 1–13, Apr. 2017.
[5] S. Maiti and J. C. Misra, "Peristaltic transport of a couple stress fluid: Some applications to hemodynamics," *J. Mech. Med. Biol.*, vol. 12, no. 3, 2012, Art. no. 1250048.
[6] R. N. Pralhad and D. H. Schultz, "Modeling of arterial stenosis and its applications to blood diseases," *Math. Biosciences*, vol. 190, no. 2, pp. 203–220, Aug. 2004.
[7] D. Tripathi, "Peristaltic flow of couple-stress conducting fluids through a porous channel: Applications to blood flow in the micro-circulatory system," *J. Biol. Syst.*, vol. 19, no. 03, pp. 461–477, Sep. 2011.
[8] A. R. Hadjesfandiari and G. F. Dargush, "Couple stress theories: Theoretical underpinnings and practical aspects from a new energy perspective," 2016, *arXiv:1611.10249*. [Online]. Available: https://arxiv.org/abs/1611.10249
[9] D. Tripathi, "Peristaltic hemodynamic flow of couple-stress fluids through a porous medium with slip effect," *Transp. Porous Media*, vol. 92, no. 3, pp. 559–572, Apr. 2012.
[10] M. Devakar, D. Sreenivasu, and B. Shankar, "Analytical solutions of couple stress fluid flows with slip boundary conditions," *Alexandria Eng. J.*, vol. 53, no. 3, pp. 723–730, Sep. 2014.
[11] G. Ramanaiah, "Squeeze films between finite plates lubricated by fluids with couple stress," *Wear*, vol. 54, no. 2, pp. 315–320, Jun. 1979.
[12] M. Ramzan, M. Farooq, A. Alsaedi, and T. Hayat, "MHD three-dimensional flow of couple stress fluid with newtonian heating," *Eur. Phys. J. Plus*, vol. 128, no. 5, pp. 1–15, May 2013.
[13] R. Devi and A. Mahajan, "Global stability for thermal convection in a couple-stress fluid," *Int. Commun. Heat Mass Transf.*, vol. 38, no. 7, pp. 938–942, Aug. 2011.
[14] J. C. Umavathi, J. P. Kumar, and A. J. Chamkha, "Convective flow of two immiscible viscous and couple stress permeable fluids through a vertical channel," *Turkish J. Eng. Environ. Sci.*, vol. 33, no. 4, pp. 221–244, 2010.

[15] S. P. Chippa and M. Sarangi, "Elastohydrodynamically lubricated finite line contact with couple stress fluids," *Tribol. Int.*, vol. 67, pp. 11–20, Nov. 2013.

[16] A. Alsaedi, N. Ali, D. Tripathi, and T. Hayat, "Peristaltic flow of couple stress fluid through uniform porous medium," *Appl. Math. Mech.*, vol. 35, no. 4, pp. 469–480, Apr. 2014.

[17] H. Basha, G. J. Reddy, and M. G. Reddy, "Chemically reactive species of time-dependent natural convection couple stress fluid flow past an isothermal vertical flat plate," *Can. J. Phys.*, vol. 97, no. 2, pp. 166–175, Feb. 2019.

[18] M. Gnaneswara Reddy, K. Venugopal Reddy, and O. D. Makinde, "Hydromagnetic peristaltic motion of a reacting and radiating couple stress fluid in an inclined asymmetric channel filled with a porous medium," *Alexandria Eng. J.*, vol. 55, no. 2, pp. 1841–1853, Jun. 2016.

[19] M. Awais, S. Saleem, T. Hayat, and S. Irum, "Hydromagnetic couple-stress nanofluid flow over a moving convective wall: OHAM analysis," *Acta Astronautica*, vol. 129, pp. 271–276, Dec. 2016.

[20] O. Makinde and A. Eegunjobi, "Entropy generation in a couple stress fluid flow through a vertical channel filled with saturated porous media," *Entropy*, vol. 15, no. 12, pp. 4589–4606, Oct. 2013.

[21] M. Farooq, S. Islam, M. T. Rahim, and A. M. Siddiqui, "Laminar flow of couple stress fluids for Vogels model," *Sci. Res. Essays*, vol. 7, no. 33, pp. 2936–2961, 2012.

[22] T. Hayat, M. Mustafa, Z. Iqbal, and A. Alsaedi, "Stagnation-point flow of couple stress fluid with melting heat transfer," *Appl. Math. Mech.*, vol. 34, no. 2, pp. 167–176, Feb. 2013.

[23] M. Dalir and M. Bashour, "Applications of fractional calculus," *Appl. Math. Sci.*, vol. 4, no. 21, pp. 1021–1032, 2010.

[24] L. Debnath, "Recent applications of fractional calculus to science and engineering," *Int. J. Math. Math. Sci.*, vol. 2003, no. 54, pp. 3413–3442, 2003.

[25] M. S. Tavazoei, M. Haeri, S. Jafari, S. Bolouki, and M. Siami, "Some applications of fractional calculus in suppression of chaotic oscillations," *IEEE Trans. Ind. Electron.*, vol. 55, no. 11, pp. 4094–4101, Nov. 2008.

[26] J. Lai, S. Mao, J. Qiu, H. Fan, Q. Zhang, Z. Hu, and J. Chen, "Investigation progresses and applications of fractional derivative model in geotechnical engineering," *Math. Problems Eng.*, vol. 2016, pp. 1–15, 2016.

[27] D. R. Anderson and D. J. Ulness, "Properties of the Katugampola fractional derivative with potential application in quantum mechanics,"*J. Math. Phys.*, vol. 56, no. 6, 2015, Art. no. 063502.

[28] E. F. D. Goufo, "Chaotic processes using the two-parameter derivative with non-singular and non-local kernel: Basic theory and applications," *Chaos: Interdiscipl. J. Nonlinear Sci.*, vol. 26, no. 8, 2016, Art. no. 084305.

[29] R. L. Magin, "Fractional calculus in bioengineering, Part3," *Crit. Rev. Biomed. Eng.*, vol. 32, nos. 3–4, pp. 195–377, 2004.

[30] M. Caputo and M. Fabrizio, "A new definition of fractional derivative without singular kernel," *Prog. Fractional Differ. Appl.*, vol. 1, no. 2, pp. 1–13, 2015.

[31] M. Caputo and M. Fabrizio, "Applications of new time and spatial fractional derivatives with exponential kernels," *Prog. Fractional Differentiation Appl.*, vol. 2, no. 1, pp. 1–11, Jan. 2016.

[32] S. Akhtar, "Flows between two parallel plates of couple stress fluids with time-fractional caputo and caputo-fabrizio derivatives," *Eur. Phys. J. Plus*, vol. 131, no. 11, pp. 1–13, Nov. 2016.

[33] M. Arif, F. Ali, N. Sheikh, and I. Khan, "Fractional model of couple stress fluid for generalized couette flow: A comparative analysis of Atangana–Baleanu and Caputo–Fabrizio fractional derivatives," *IEEE Access*, vol. 7, pp. 88643–88655, 2019.

[34] M. Arif, F. Ali, I. Khan, and K. S. Nisar, "A time fractional model with non-singular kernel the generalized couette flow of couple stress nanofluid," *IEEE Access*, vol. 8, pp. 77378–77395, 2020.

[35] N. A. Sheikh, F. Ali, and I. Khan, "A modern approach of Caputo–Fabrizio time-fractional derivative to MHD free convection flow of generalized second-grade fluid in a porous medium," *Neural Comput. Appl.*, vol. 30,pp. 1865–1875, Dec. 2018.

[36] F. Ali, M. Saqib, and I. Khan, "Application of Caputo-Fabrizio derivatives to MHD free convection flow of generalized Walters'-B fluid model," *Eur. Phys. J. Plus*, vol. 131, p. 377, Oct. 2016.

[37] M. A. Imran, M. Aleem, M. B. Riaz, R. Ali, and I. Khan, "A comprehensive report on convective flow of fractional (ABC) and (CF) MHD viscous fluid subject to generalized boundary conditions," *Chaos, Solitons Fractals*, vol. 118, pp. 274–289, Jan. 2019.

[38] M. Ahmad, M. A. Imran, M. Aleem, and I. Khan, "A comparative study and analysis of natural convection flow of MHD non-newtonian fluid in the presence of heat source and first-order chemical reaction," *J. Thermal Anal. Calorimetry*, vol. 137, no. 5, pp. 1783–1796, Sep. 2019.

[39] I. Khan, M. Saqib, and F. Ali, "Application of time-fractional derivatives with non-singular kernel to the generalized convective flow of casson fluid in a microchannel with constant walls temperature," *Eur. Phys. J. Special Topics*, vol. 226, nos. 16–18, pp. 3791–3802, Dec. 2017.

[40] J. C. Maxwell, *A Treatise on Electricity and Magnetism*. Oxford, U.K.: Clarendon Press, 1881.

[41] S. U. Choi and J. A. Eastman, "Enhancing thermal conductivity of fluids with nanoparticles," Argonne Nat. Lab., Lemont, IL, USA, Tech. Rep. ANL/MSD/CP-84938; CONF-951135-29, 1995.

[42] M. G. Reddy, A. H. Seikh, M. V. V. N. L. Sudharani, M. Rahimi-Gorji, and N. Alharthi, "Dusty flow with different water based nanoparticles along a paraboloid revolution: Thermal analysis," *Microsyst. Technol.*, vol. 26, no. 3, pp. 925–945, Mar. 2020.

[43] M. Arif, F. Ali, N. A. Sheikh, and I. Khan (2019), "Enhanced heat transfer in working fluids using nanoparticles with ramped wall temperature: Applications in engine oil," Advances in Mechanical Engineering, vol. 11, no. 11, pp. 1–11, 2019.

[44] F. Ali, S. Murtaza, I. N. A. Khan Sheikh, and K. S. Nisar, "Atangana–Baleanu fractional model for the flow of Jeffrey nanofluid with diffusion-thermo effects: Applications in engine oil," *Adv. Difference Equ.*, vol.2019, p. 346 , Aug. 2019.

[45] O. Mahian, A. Kianifar, S. A. Kalogirou, and I. S. Pop Wongwises, "A review of the applications of nanofluids in solar energy," *Int. J. Heat Mass Transf.*, vol. 57, no. 2, pp. 582–594, 2013.

[46] K. V. Wong and O. De Leon, "Applications of nanofluids: Current and future," *Adv. Mech. Eng.*, vol. 2, Mar. 2010, Art. no. 519659.

[47] S. Senthilraja, M. Karthikeyan, and R. Gangadevi, "Nanofluid applications in future automobiles: Comprehensive review of existing data," *Nano-Micro Lett.*, vol. 2, no. 4, pp. 306–310, Dec. 2010.

[48] L. Pislaru-Danescu, A. M. Morega, G. Telipan, M. Morega, J. B. Dumitru, and V. Marinescu, "Magnetic nanofluid applications in electrical engineering," *IEEE Trans. Magn.*, vol. 49, no. 11, pp. 5489–5497, Nov. 2013.

[49] A. Rufus, N. Sreeju, and D. Philip, "Synthesis of biogenic hematite (α-Fe_2O_3) nanoparticles for antibacterial and nanofluid applications," *RSC Adv.*, vol. 6, no. 96, pp. 94206–94217, 2016.

[50] M. Rafati, A. A. Hamidi, and M. Shariati Niaser, "Application of nanofluids in computer cooling systems (heat transfer performance of nanofluids)," *Appl. Thermal Eng.*, vols. 45–46, pp. 9–14, Dec. 2012.

[51] M. Zhang, X. Wang, W. Liu, and X. Fu, "Performance and anti-wear mechanism of Cu nanoparticles as lubricating oil additives," *Ind. Lubrication Tribol.*, vol. 24, no. 55, pp. 347–357, 2009.

[52] M. Zhang, X. Wang, W. Liu, and X. Fu, "Performance and anti-wear mechanism of Cu nanoparticles as lubricating oil additives," *Ind. Lubrication Tribol.*, vol. 24, no. 130, pp. 78–89, 2009.

[53] S. Zeinali Heris, M. Nasr Esfahany, and S. G. Etemad, "Experimental investigation of convective heat transfer of Al2O3/water nanofluid in circular tube," *Int. J. Heat Fluid Flow*, vol. 28, no. 2, pp. 203–210, Apr. 2007.

[54] F. Aamina, I. Khan, and N. Sheikh Muhammad Saqib, "Magnetohydrodynamic flow of brinkman-type engine oil based MoS2-nanofluid in a rotating disk with Hall effect," *Int. J. Heat Technol.*, vol. 35, no. 4, pp. 893–902, Dec. 2017.

[55] S. A. A. Jan, F. Ali, N. A. Sheikh, I. S. M. Khan, and M. Gohar, "Engine oil based generalized brinkman-type nano-liquid with molybdenum disulphide nanoparticles of spherical shape: Atangana-Baleanu fractional model," *Numer. Methods Partial Differ. Equ.*, vol. 34, no. 5, pp. 1472–1488, 2018.

[56] F. A. Aamina, I. Khan, N. A. Sheikh, M. Gohar, and I. Tlili, "Effects of different shaped nanoparticles on the performance of engine-oil and kerosene-oil: A generalized brinkman-type fluid model with non-singular kernel," *Sci. Rep.*, vol. 8, no. 1, pp. 1–13, Dec. 2018.

[57] F. Ali, F. Ali, N. A. Sheikh, I. Khan, and K. S. Nisar, "Caputo–Fabrizio fractional derivatives modeling of transient MHD Brinkman nanoliquid: Applications in food technology," *Chaos, Solitons Fractals*, vol. 131, Feb. 2020, Art. no. 109489.

[58] F. A. Aamina, I. Khan, N. A. Sheikh, M. Gohar, and I. Tlili, "Effects of different shaped nanoparticles on the performance of engine-oil and kerosene-oil: A generalized brinkman-type fluid model with non-singular kernel," *Sci. Rep.*, vol. 8, no. 1, pp. 1–13, Dec. 2018.

[59] N. A. Sheikh, F. Ali, and I. M. Khan Gohar, "A theoretical study on the performance of a solar collector using CeO_2 and Al_2O_3 water based nanofluids with inclined plate: Atangana–Baleanu fractional model," *Chaos, Solitons Fractals*, vol. 115, no. 1, pp. 135–142, Oct. 2018.
[60] M. Gnaneswara Reddy and M. Ferdows, "Species and thermal radiation on micropolar hydromagnetic dusty fluid flow across a paraboloid revolution," *J. Thermal Anal. Calorimetry*, to be published.
[61] M. G. Reddy, P. Vijayakumari, L. Krishna, K. G. Kumar, and B. C. Prasannakumara, "Convective heat transport in a heat generating MHD vertical layer saturated by a non-Newtonian nanofluid: A bidirectional study," *Multidiscipline Model. Mater. Struct.*, to be published.
[62] M. Devakar, D. Sreenivasu, and B. Shankar, "Analytical solutions of couple stress fluid flows with slip boundary conditions," *Alexandria Eng. J.*, vol. 53, no. 3, pp. 723–730, Sep. 2014.
[63] L. Debnath and D. Bhatta, *Integral Transforms and Their Applications*, 2nd ed. London, U.K.: Chapman & Hall, 2006.
[64] I. S. Gradshteyn and I. M. Ryzhik, *Table of Integrals, Series, and Products*, 7th ed. Amsterdam, The Netherlands: Elsevier, 2007.
[65] S. Akhtar and N. A. Shah, "Exact solutions for some unsteady flows of a couple stress fluid between parallel plates," *Ain Shams Eng. J.*, vol. 9, no. 4, pp. 985–992, Dec. 2018.

FARHAD ALI received the Ph.D. degree in applied mathematics from Universiti Teknologi Malaysia, one of the world leading Universities.

He has over 13 years of academic experience in different reputed institutions of the country. He is currently working as the Dean of the Sciences and IT, City University of Science and IT. He is also working as the Head of the Department of Mathematics. He is also the Head of the Computational Analysis Research Group, Ton Duc Thang University, Vietnam. Additionally, he has the charge of the Director ORIC. He is an HEC Approved Supervisor and has supervised dozens of M.S. scholars. Apart from academic, he has organized academic knowledge seminars and international conferences for students, faculty members, researchers, and practitioners from different parts of the world. He has published more than 100 research articles in different well-reputed international journals of the world. His research interests include fluid dynamics, MHD flows, nanofluids, fractional derivatives, integral transforms, exact solutions, and mathematical modeling.

Dr. Ali is a potential Reviewer of many research journals of the world. He is the Editor of some high-ranked journals. He is also the Chief Editor of the *City University International Journal of Computational Analysis*.

ZUBAIR AHMAD received the B.S. degree in mathematics from the University of Peshawar. He is currently pursuing the M.S. degree in applied mathematics with the Department of Mathematics, City University of Science and Information Technology, Peshawar, Pakistan, under the supervision of Associate Professor Dr. Farhad Ali (HoD Mathematics, CUSIT). His research interests include heat and mass transfer, fluid dynamics, two phase flows, MHD flows, nanofluids, couple stress fluid, fractional derivatives, integral transforms, exact solutions, and mathematical modeling.

MUHAMMAD ARIF received the M.S. degree in applied mathematics, under the supervision of Associate Professor Dr. Farhad Ali (HoD Mathematics, CUSIT), and the M.Sc. degree in mathematics from the City University of Science and Information Technology, Peshawar. He has published five research articles in different well-reputed high-impact factor international journals of the world. He has more than eight years of academic experience in different reputed institutions of the city. His most experience has been working in the academic sector. His research interests include fluid dynamics, two phase flows, MHD flows, nanofluids, couple stress fluid, fractional derivatives, integral transforms, exact solutions, numerical solutions, and mathematical modeling.

ILYAS KHAN received the Ph.D. degree in applied mathematics from Universiti Teknologi Malaysia, one of the world leading Universities.

He has over 15 years of academic experience in different reputed institutions of the world. He is currently an Associate Professor with the Department of Mathematics, Majmaah University, Saudi Arabia. He is also a Researcher associated with Ton Duc Thang University, Vietnam. He has published more than 250 research articles in different well-reputed international journals of the world. His research interests include fluid dynamics, MHD flows, nanofluids, fractional derivatives, integral transforms, exact solutions, and mathematical modeling.

Dr. Khan is the potential Reviewer of many research journals of the world.

KOTTAKKARAN SOOPPY NISAR is currently an Associate Professor with the Department of Mathematics, Prince Sattam Bin Abdulaziz University, Saudi Arabia. He has more than 150 research publications. His current research interests include special functions, fractional calculus, and SAC-OCDMA code networks.